

Probing phonon-rotation coupling in helium nanodroplets: Infrared spectroscopy of CO and its isotopomers

Klaus von Haeften,^{1,*} Stephan Rudolph,¹ Iaroslav Simanovski,^{1,†} Martina Havenith,¹
Robert E. Zillich,^{2,3,4} and K. Birgitta Whaley²

¹*Lehrstuhl für Physikalische Chemie II, Ruhr-Universität Bochum, D-44780 Bochum, Germany*

²*Department of Chemistry and Pitzer Center for Theoretical Chemistry, University of California, Berkeley, California 94720, USA*

³*Fraunhofer ITWM, 67663 Kaiserslautern, Germany*

⁴*Institut für Theoretische Physik, Johannes Kepler Universität, A-4040 Linz, Austria*

(Received 5 September 2005; revised manuscript received 15 November 2005; published 3 February 2006)

We have recorded the $R(0)\nu_{\text{CO}}=1\leftarrow 0$ IR spectrum of CO and its isotopomers in superfluid helium nanodroplets. For droplets with average size $N \geq 2000$ helium atoms, the transition exhibits a Lorentzian shaped linewidth of 0.034 cm^{-1} , indicating a homogeneous broadening mechanism. The rotational constants could be deduced and were found to be reduced to about 60% of the corresponding gas-phase values (63% for the reference $^{12}\text{C } ^{16}\text{O}$ species). Accompanying calculations of the pure rotational spectra were carried out using the method of correlated basis functions in combination with diffusion Monte Carlo (CBF/DMC). These calculations show that both the reduction of the rotational B constant and the line broadening can be attributed to phonon-rotation coupling. The reduction in B is confirmed by path integral correlation function calculations for a cluster of 64 ^4He atoms, which also reveal a non-negligible effect of finite size on the collective modes. The phonon-rotation coupling strength is seen to depend strongly on the strength and anisotropy of the molecule-helium interaction potential. Comparison with other light rotors shows that this coupling is particularly high for CO. The CBF/DMC analysis shows that the $J=1$ rotational state couples effectively to phonon states, which are only present in large helium droplets or bulk. In particular, they are not present in small clusters with $n \leq 20$, thereby accounting for the much narrower linewidths and larger B constant measured for these sizes.

DOI: [10.1103/PhysRevB.73.054502](https://doi.org/10.1103/PhysRevB.73.054502)

PACS number(s): 67.40.Yv, 36.20.Ng, 36.40.Gk, 05.30.Jp

I. INTRODUCTION

Bulk superfluid helium exhibits a manifold of unusual phenomena.¹ These include the possibility of exciting collective elementary excitations such as phonons, rotons, and quantized circulation (vortices). The phonon and roton branch in liquid helium was predicted very early by Landau^{2,3} and later confirmed by inelastic neutron scattering experiments.⁴ The existence of quantum vortices, i.e., quantized rotational excitations, is a striking manifestation of superfluidity.⁵ Following the experimental realization of Bose-Einstein condensates (BEC),⁶ the special properties of finite size Bose condensates became a topic of interest for the scientific community. One important goal here is the study of general properties of condensates, such as their collective excitations.⁷⁻⁹ Experimental measurements of collective excitation modes can provide a tool to probe superfluidity. The detection of vortices in BECs (Refs. 10-12) was the experimental evidence confirming superfluidity. Investigation of volume compressional modes (phonons) is now well established as a means of gaining insight into the physical behavior of ultracold quantum gases in different regimes of Bose and Fermi gas.^{7,8,13}

Helium nanodroplets constitute a related prototype of finite size quantum fluids.¹⁴⁻¹⁶ The quantum nature of the dilute Bose gas shows up at temperatures where the Broglie wavelength becomes larger than the spacing between individual particles. The Bose particles will then lose their identity and can be considered as a single macroscopic wave function. Just as in BECs, the finite size of helium nanodrop-

lets leads to a discrete collective excitation spectrum which depends on the cluster size.^{17,18} Due to their inherent spherical symmetry, volume excitation modes of helium nanodroplets are described by radial nodes and describe density fluctuations with a wavelength smaller or equal to the cluster radius R . This spectrum evolves from a small number of discrete excitations for small clusters to a spectrum resembling the phonon-roton branch in liquid bulk helium for large droplets.^{17,18} The observation of a phonon side band in the electronic spectrum of glyoxal embedded in helium nanodroplets established evidence for coupling between a chromophore and elementary excitations of the droplet.¹⁹ Babichenko and Kagan considered the particular case of coupling between molecular rotations and phonons in order to explain the different linewidths in the rovibrational spectrum of OCS in ^3He and ^4He droplets.²⁰ Later, Nauta and Miller referred to possible coupling between molecular rotation and excitation of the liquid as the origin of homogeneous broadening.²¹ We report here an infrared study which gives a direct experimental evidence for the coupling of these quantized volume compressional modes in helium nanodroplets with a single rotating dopant diatomic molecule that is embedded inside the helium nanodroplet. The rotating molecular dopant serves as the spectroscopic probe inside the helium droplet. The magnitude of the coupling is shown to depend on the anisotropy of the interaction potential between the molecular dopant and the helium, on the accessible density of states as provided by the helium excitation spectrum, and on the moment of inertia of the dopant.

It has been demonstrated in the past that the superfluid nature of helium droplets allows the study of rotationally

resolved spectra of a molecule within this finite size quantum fluid,^{22–24} providing experimental access to their special properties. The measurement of vibrational-rotational spectra allows determination of the rotational energies and hence the effective moment of inertia of a molecule in the helium droplets. Several systematic trends have been established from many experimental studies over the last ten years. For heavy molecules a considerable increase in the moment of inertia has been found,^{22,25} corresponding to a decrease in the rotational constant. This has been explained by the adiabatic following of a molecule induced nonsuperfluid fraction of the solvation shell.^{15,26}

In contrast, it has been found that lighter molecules such as HCN and HCCH show a much smaller reduction of their rotational constant in ⁴He droplets. The rotational constant of HCN is reduced to 79% of the gas phase value ($B_0 = 1.478 \text{ cm}^{-1}$), while the rotational constant of HCCH ($B_0 = 1.1766 \text{ cm}^{-1}$ in gas phase) is reduced to 88%.^{21,27} The smaller reduction of the light dopants has been attributed to a breakdown of adiabatic following of helium, as a result of the high rotational velocities of light molecules.²⁸ Theoretical work has shown that for light molecules, instead of coupling to the localized helium solvation layers, where the superfluid fraction is reduced, an appreciable coupling to delocalized collective helium modes is to be expected.²⁹ In particular, rotational states of the molecule which lie close to the roton excitation energy of ⁴He will couple strongly to the high density of states in the roton regime. Such rotation-roton coupling has been predicted to give rise to an anomalously large effective distortion constant for a linear molecule, and has been demonstrated to account quantitatively for the value measured recently for HCCH.³⁰

Diatomic molecules are ideal candidates to investigate the coupling between rotational excitation and collective modes of ⁴He droplets, because they possess only a single vibrational mode. Due to the vastly different energy scales between rotational excitations and the vibrational mode of the diatom, the vibrational degree of freedom essentially decouples from the rotational degree of freedom. Therefore, coupling to vibrational states can be excluded. We have chosen CO as our prototype diatomic, since the rotational energies of CO isotopomers lie in a particularly interesting energy range between the long-wavelength phonons and the rotons of superfluid ⁴He.

The spectroscopy of CO molecules in large ⁴He droplets studied here will be seen to show quite different results from recent studies of CO in small helium clusters. IR spectra of small clusters of ¹²C ¹⁶O-He_N, ¹³C ¹⁶O-He_N, and ¹²C ¹⁸O-⁴He_N ($N \leq 20$) have recently been reported by Tang and McKellar.^{31,32} Their spectra show the evolution of line frequencies as a function of cluster size up to the first and partly filled second solvation layer. In the present work we shall show that there exist qualitative differences between the spectra in such small clusters and in large droplets. We provide an explanation for these differences in terms of the coupling of the rotational motion of the dopant to the collective excitations of the helium droplet and size dependent features of the latter.

The current study provides a direct experimental test of predicted coupling between rotational motion of a linear

molecule and collective excitations of helium. Our analysis employs theoretical calculations for the spectra that allow both the rotational constant and the linewidth to be estimated. CO is an attractive model system for theoretical studies of molecule-helium cluster interactions since accurate potential interaction surfaces exist^{33,34} and the energy level description is quite simple. Several calculations have addressed the structural or dynamical properties of CO in small clusters.^{34–38} The dynamics in large droplets is analyzed here using the recently developed combination of correlated basis function theory and diffusion Monte Carlo simulations (CBF/DMC),²⁹ as well as the path integral correlation function approach (PICF).³⁸ We will discuss the effects of cluster size and show that an analysis of the coupling to helium density beyond the first solvation shell is necessary for a full understanding of the way in which the molecular rotational spectra change on going from small helium clusters to large helium nanodroplets.

II. EXPERIMENTAL AND THEORETICAL METHODS

A. Experiment

We have set up a molecular beam machine in Bochum for the IR spectroscopy of dopants in helium nanodroplets. The pick-up-technique serves to dope the droplets with foreign molecules.³⁹ Absorption of photons is detected by beam depletion using an electron impact quadrupole mass spectrometer.⁴⁰ The experimental set up is quite similar in principle to that described by Hartmann *et al.*⁴⁰

Our molecular beam apparatus consists of four vacuum chambers: The first chamber carries the cluster source, operated at 10–20 K using liquid He as a coolant. The He gas flows at room temperature through a 3 mm pipe directly into a home made heat exchanger that is mounted at the end of the cold head (modified ST-100, Janis). A 2 μm porous filter kept at low temperatures prevents the nozzle from clogging by small amounts of foreign impurities. After the filter, the He gas expands into vacuum through a 5 μm nozzle (Pt/Ir) sealed with a thin washer (0.15 mm) of indium. The temperature can be adjusted using a needle valve in the liquid He transfer line and an electrical heater inside the cryostat. A controller is used to stabilize the temperature with an accuracy of 0.1 K. The overall length of the nozzle assembly between the head of the cold finger and the orifice is 60 mm. The heat exchanger is made of ultrapure copper (99.999 %, annealed) which has a high heat conductance of $135 \text{ W cm}^{-1} \text{ K}^{-1}$ at a temperature of 20 K. The nozzle assembly is separately shielded from heat radiation and the whole cryostat resides within an outer heat shield that is sunk at 80 K. With these two shields the cryostat can reach a temperature of 3.7 K without any gas load. At a He pressure of 40 bar the minimum temperature is 5 K.

For a fixed stagnation pressure of $p_0 = 40$ bar and a nozzle diameter $d_0 = 5 \mu\text{m}$, the average size \bar{N} of the droplets will depend on the nozzle temperature T_0 . The associated cluster sizes are obtained by comparison to reference values from scattering experiments reported in the literature.⁴¹ The sizes of the droplets are distributed over a wide range, character-

ized by a log-normal dependence. For a mean size of the droplets \bar{N} , the width is roughly $\sqrt{\bar{N}}$.⁴² For $T_0=20$ K, we have $\bar{N}=2600$ atoms.

Due to the rather high gas load the first chamber is equipped with a baffled 8000 l/s diffusion pump with an actual pumping speed of ~ 4500 l/s. 20 mm downstream from the nozzle the droplet beam has to pass through a 0.5 mm skimmer into a 40 mm long pick-up chamber that is pumped by a 50 l/s turbo molecular pump. CO is used as a dopant. The effective path length for pick-up is slightly longer than 60 mm, taking into account the length of the skimmer and the 6 mm large exit aperture of the pick-up chamber. The He partial pressure is typically about 10^{-6} mbar. A differential pumping scheme is applied using a 2000 l/s diffusion pump. The droplets enter through a 3 mm aperture into a chamber containing a mass spectrometer. The ionization region is 1250 mm behind the nozzle. The chamber is evacuated by a 50 l/s turbo molecular pump. The typical base pressure after heating at 150 °C is 1×10^{-10} mbar. For the detection we used a Pfeiffer-QMA 400 quadrupole-mass spectrometer with a mass range from 1 to 1064 amu. Absorption is detected via depletion of the mass spectrometer signal caused by the reduction of the droplet size after excitation of the dopant molecule. The method relies on efficient energy transfer from the excited molecule to the droplet, followed by the evaporation of several hundred He atoms.⁴⁰ For CO in He droplets, however, the situation is somewhat special. When embedded in liquid argon or nitrogen, vibrationally excited CO exhibits long lifetimes, equal to 18.2 and 19.6 ms, respectively.^{43,44} Moreover, the main relaxation channel is radiative. Nonradiative decay is expected to be slower than 1.5 s.^{44,45} However, Lindsay and Miller have demonstrated that for the similar case of HF in He droplets, depletion is achieved via the pick up of a second molecule. This results in aggregation to form an embedded complex that can relax via additional low lying vibrational modes.⁴⁶ We expect the same mechanism to hold for CO. Furthermore, we point out that although a complex is formed, it is feasible to detect infrared absorption of single CO molecules. Inside the pick-up chamber the partial pressure of CO is two to three orders of magnitude higher than the background pressure. The probability of forming a complex by pick-up of a, e.g., water molecule in addition to a single CO molecule increases as the CO doped droplet travels downstream towards the mass spectrometer. It becomes significant far from the nozzle and pick-up chamber, in a region where the overlap between droplet and laser beam is much lower than close to the pick-up chamber.

Scans were taken at different CO partial pressures. Figure 1 displays mass spectra both for pure and for doped droplets at a CO pick-up pressure of 5×10^{-6} mbar, 1.5×10^{-5} mbar and 1×10^{-4} mbar, respectively. The mass spectrum of pure ^4He droplets shows maxima at 4 amu, 8 amu, 12 amu, etc., which are attributed to the He monomer, dimer, trimer, etc. It has been shown before that the mass spectrum of pure He droplets reflects the products of their fragmentation rather than their initial size or structure.⁴⁷ The peaks at 1, 2 and 18 amu are an exception to this. These peaks are assigned to H^+ , H_2^+ , and H_2O^+ , resulting from residual H_2O captured by the droplets.

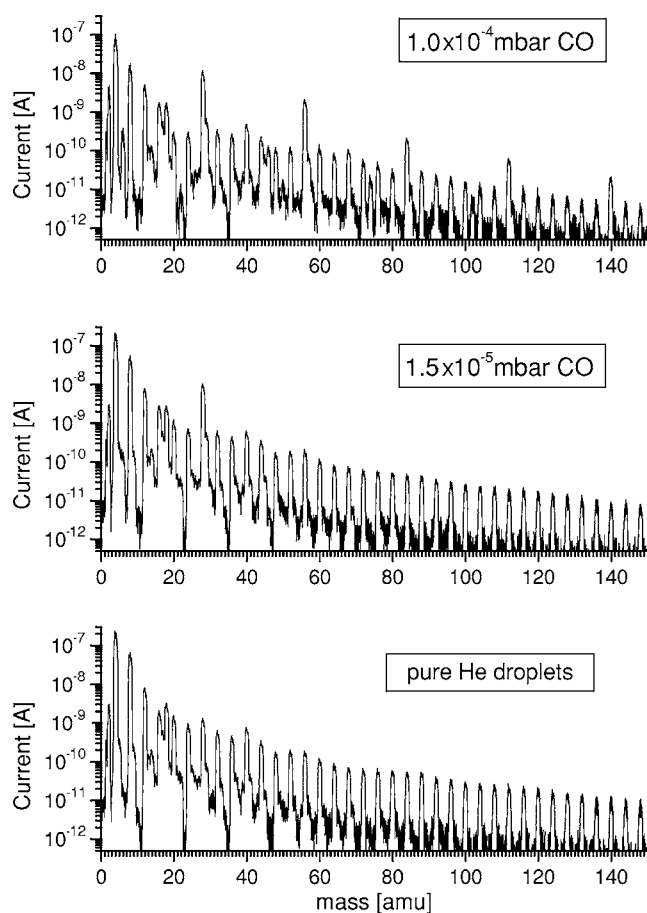


FIG. 1. Mass spectra of pure and CO doped ^4He droplets taken at different CO partial pressures in the pick-up chamber. The multiplier voltage is 1400 V, corresponding to a current amplification of 3500. The mean size of the droplets is 2600 atoms. Pure He droplets reveal a mass spectrum of lines decreasing in intensity to some hundred amu, reflecting the fragmentation process. For the doped droplets the peaks at 28, 56, 84, ... gain in intensity. These peaks result from the ionization of embedded CO monomers, dimers, trimers, etc.

CO doped He droplets show a mass spectrum with a distinct peak at 28 amu (1.0×10^{-8} A). In this case the charge localization process takes place preferably at the dopant molecule, due to the lower ionization threshold compared to that of He.⁴⁷

When increasing the partial pressures of CO, the droplets are likely to pick up more than one CO molecule, favoring aggregation.^{48,49} As shown in Fig. 1, CO dimers, trimers, tetramers, and pentamers can be observed at masses 56, 84, 112, and 140 amu, respectively, for CO partial pressures of 1.0×10^{-4} mbar. The intensity distribution of the latter peaks follows a Poisson function of the pick up pressure, while the monomer intensity dependence rises monotonically, indicating fragmentation of higher complexes upon ionization.⁴⁸ Based upon these data we have deduced the cross section for picking up and embedding a CO molecule inside a He droplet of size $N \sim 2600$ atoms to be 3000 \AA^2 , which is close to the geometric cross section of a He droplet of $N=2600$.⁴⁸

We observe additional peaks at 29, 57, 85, 112, and 141 amu. These peaks are attributed to protonated CO molecules

that originate from CO-H₂O van der Waals complexes either in their ground or vibrationally excited states after electron impact of the He droplet. We assume that CO molecules in He droplets have long-lived vibrational states (>1 ms) similar to what is observed in liquid nitrogen.⁴⁴ The vibrational relaxation rates of CO*-H₂O complexes are expected to be much shorter than 1 ms.⁵⁰ We therefore conclude that the formation of CO*-H₂O complexes result in a faster relaxation via low lying intermolecular vibrations which might be essential for the detection of infrared absorption by depletion.⁴⁶

The infrared diode laser setup has been described previously.^{51,52} Three different laser diodes are used. Frequency tuning is achieved by a continuous change of the current through the laser diode while the temperature is kept constant by a homemade PID controller.

The divergent laser radiation is coupled out via 3 spherical mirrors that provide a parallel beam of ~ 20 mm in diameter. The laser beam is directed over a distance of 4 m to a focusing mirror ($f=2$ m) in front of the molecular beam machine and coupled in through a calcium fluoride window. We use an antiparallel arrangement. Inside the molecular beam machine the laser light crosses the ionization region of the quadrupole mass spectrometer and continues along the droplet path to the nozzle. The focal point lies close to the skimmer inside the pick-up chamber.

For frequency calibration outside the machine, part of the laser light is coupled out by a beam splitter and directed to a monochromator. The laser beam is then split and directed into a reference cell and a confocal etalon. The reference cell has been filled with 13 mbar N₂O. The spectral data are linearized and calibrated by the well-known absorption lines of N₂O gas (Ref. 53) and the 300 MHz spaced marker lines of an etalon.

We used phase-sensitive detection by a lock-in amplifier with the laser beam chopped at 29 Hz which yielded the optimal signal to noise ratio. The integration time of the lock-in amplifier was 3 s and the filter slope was set to 6 dB/octave.

B. Theory

For calculation of the absorption spectrum of CO in helium we employ here both the CBF/DMC method, which combines correlated basis function theory with diffusion Monte Carlo simulations, and the path integral correlation function approach. In Ref. 29 two of us have developed the CBF formulation for rotational excitation of linear molecules in bulk superfluid helium and combined it with DMC for the calculation of ground state properties needed for CBF. We have shown^{29,30} that the CBF/DMC method yields rotational constants for the light rotors HCN and HCCH in bulk helium that are in good agreement with values derived from experimental rovibrational spectra in large helium droplets. Since CO is similar to HCN and HCCH and high quality interaction potentials are also available for CO, we expect to achieve a similarly good agreement for CO here. Furthermore, CBF is able to obtain not only transition energies, but also to provide predictions for the spectral linewidths. This

makes CBF/DMC the method of choice for investigating the large linewidth observed for CO in large helium droplets.

Despite these positive characteristics, the CBF/DMC method does not necessarily predict exact rotational spectra, because of its restriction to time-dependent particle densities and pair distributions, but not higher order distributions, as well as other systematic approximations.²⁹ Therefore, we have also performed path integral Monte Carlo (PIMC) simulations and used the PICF approach to calculate the rotational spectra in finite clusters.³⁸ This method provides a finite temperature calculation free from systematic approximations and allows investigation of the size dependence of the absorption spectrum and rotational constants. In the PICF method, the equilibrium average of an imaginary time correlation function—in the case of the rotational absorption spectrum, the orientational auto-correlation function—is calculated using the molecule helium Hamiltonian that includes molecular rotation³⁸ and all translational degrees of freedom as well as the exchange symmetry of helium.⁵⁸ Given sufficient sampling (small error bars) and a spectrum which is “not too complicated” (i.e., few well-separated lines), these imaginary time auto-correlation functions can be numerically transformed to real frequency to obtain the absorption spectrum. The required inverse Laplace transform is made here with the maximum entropy method according to the formulation of Bryan.⁵⁹ Calculations are carried out at temperature $T=0.625$ K. This is almost twice as high as the temperature observed experimentally in ⁴He droplets,⁴⁰ but at a cluster size of $N=64$ ⁴He atoms, all relevant properties of the cluster are found to be insensitive to temperature variations below 1 K. Full methodological details are presented elsewhere.³⁸

The droplets studied in our experiment consist of up to a few thousand ⁴He atoms and have a radius on the order of 30 Å, which is still microscopic. The droplet properties are certainly not fully converged to the bulk limit. In particular, the spectrum of volume excitations is expected to be still discrete (see, e.g., Fig. 1 of Ref. 54), although key features such as the roton excitation are already well-established at this size.^{17,18} Since the ⁴He excitation spectrum is a crucial ingredient of the CBF theory of molecular rotations in helium, one has to be very careful when applying the results of bulk calculations to finite droplets. We will come back to this important point in section II B 2 below and also in the discussion of experimental and theoretical results in Section IV.

1. CBF/DMC method

We give here an overview of essential features of the CBF/DMC method. The first step is a DMC simulation, with the interaction potentials between CO and ⁴He (Ref. 33) and between ⁴He and ⁴He (Ref. 55) as the only input. As in Refs. 29 and 30 we employ periodic boundary conditions for the DMC simulation. The cubic simulation box contains $N=256$ atoms and has a side length of $s=23$ Å. s was adjusted such that equilibrium density was reached at the edge of the box. The finite box side length s limits the results for the linewidth, as discussed below. The DMC simulation provides an unbiased⁵⁶ pair distribution function $g(r, \cos \theta)$, where \mathbf{r} is the vector between ⁴He and the center of mass of CO, and θ is the angle between the orientation Ω of the CO axis and

r. In the second step, the pure rotational spectrum $S_J(\omega)$ of CO in bulk ${}^4\text{He}$ for the transition $0 \rightarrow J$ is obtained with the CBF theory²⁹

$$S_J(\omega) = \text{Im}[\hbar\omega - B_0J(J+1) - \Sigma_J(\omega)]^{-1} \\ = \frac{\text{Im}\Sigma_J(\omega)/\pi}{(\gamma_J(\omega) - \hbar\omega)^2 + [\text{Im}\Sigma_J(\omega)]^2}, \quad (2.1)$$

where we have defined $\gamma_J(\omega) = B_0J(J+1) + \text{Re}\Sigma_J(\omega)$. $\Sigma_J(\omega)$ is

the ‘‘self-energy’’ of the linear molecule in the rotational state of total angular momentum J coupling to elementary excitations $\epsilon(k)$ of the ${}^4\text{He}$ environment (Fig. 2). The self-energy $\Sigma_J(\omega)$ is complex and depends on the energy $\hbar\omega$. It is given by

$$\Sigma_J(\omega) = - \int dk \sigma_J(\omega, k), \quad (2.2)$$

where we have defined the self-energy density

$$\sigma_J(\omega, k) = B_0^2 \frac{(4\pi)^2 \rho}{2J+1} \sum_{\ell} \frac{1}{(2\pi)^3} \frac{k^2}{S(k)} \frac{\sum_{\ell'} \tilde{L}(J, \ell', \ell) g_{\ell'}^2(k)}{B_0 \ell(\ell+1) + \epsilon(k) + \hbar^2 k^2 / 2M - \hbar\omega}, \quad (2.3)$$

with ρ the He density, M the mass of the molecule, and $g_{\ell'}(k)$ the Bessel transform of the Legendre expansion coefficient $g_{\ell'}(r)$ of the pair distribution function $g(r, \cos \theta)$ that was obtained in a first step with diffusion Monte Carlo:

$$g(r, \cos \theta) - 1 = 4\pi \sum_{\ell} (2\ell+1) P_{\ell}(\cos \theta) \int \frac{dk k^2}{(2\pi)^3} j_{\ell}(kr) g_{\ell}(k). \quad (2.4)$$

Here P_{ℓ} are the Legendre polynomials. The other quantities in $\Sigma_J(\omega)$, namely the phonon-roton spectrum $\epsilon(k)$ and the static structure factor $S(k)$, can be obtained from experimental data on bulk liquid He, see Ref. 29. $\tilde{L}(J, \ell', \ell)$ enforces dipole selection rules and is also defined in Ref. 29. The energy denominator in Eq. (2.3) indicates the mechanism by which the rotational energy is reduced: rotational motion of energy $\hbar\omega$ can couple to other rotational modes of energy $B_0 \ell(\ell+1)$ by excitation of collective helium modes of energy $\epsilon(k)$ and molecular translation $\hbar^2 k_{\text{mol}}^2 / 2M$ (recoil). Linear and angular momentum and, in the case of a decay process, energy are conserved,

$$\hbar\omega = B_0 \ell(\ell+1) + \epsilon(k) + \hbar^2 k_{\text{mol}}^2 / 2M,$$

$$\mathbf{k} = \mathbf{k}_{\text{mol}},$$

$$\delta(J, \ell', \ell) = 1,$$

where $\delta(J, \ell', \ell) = 1$ signifies the ‘‘triangle condition,’’ i.e., that J, ℓ', ℓ can form a triangle.

The form of Eq. (2.1) suggests that for a small value of the imaginary part of the self-energy, $\text{Im}\Sigma_J(\omega)$, the spectrum $S_J(\omega)$ is a Lorentzian centered at ω' and with width Δ :

$$S_J(\omega) \approx \frac{1}{\pi} \frac{\Delta}{(\hbar\omega - \hbar\omega')^2 + \Delta^2}. \quad (2.5)$$

Here the width Δ is given by $\Delta = \text{Im}\Sigma_J(\omega')$. This expression is valid for ω in the proximity of the peak located at ω' . The

peak location, ω' is determined by solving the equation $\gamma_J(\omega) - \hbar\omega = 0$. Hence Δ is the homogeneous linewidth (FWHM/2) resulting from all possible decays into lower states $J \rightarrow J-1, J-2, \dots$, that are accompanied by excitation of helium modes.

To calculate the homogeneous linewidth Δ of the $J=1$ state, we can use the expression for the self-energy, Eqs. (2.2) and (2.3), obtaining

$$\Delta \equiv \text{Im}\Sigma_{J=1}(\omega') = \frac{2}{3} B_0^2 \rho \frac{k_0^2}{S(k_0)} \frac{\tilde{L}(1, 1, 0) g_1^2(k_0)}{d\epsilon(k_0)/dk + \hbar^2 k_0 / M}, \quad (2.6)$$

where k_0 is the wave vector of the phonon which is excited by the decay. k_0 is obtained by solving the equation

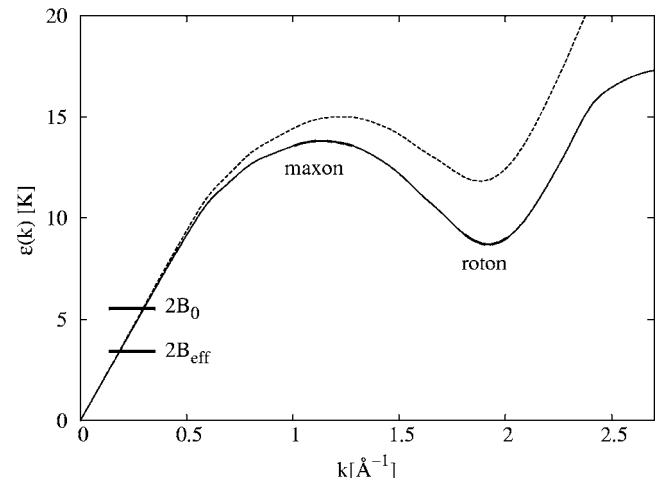


FIG. 2. The experimental phonon-roton spectrum $\epsilon(k)$ of bulk ${}^4\text{He}$ (Ref. 4) (full line) and the helium spectrum plus molecular recoil energy, $\epsilon(k) + \hbar^2 k^2 / 2M$, (dashed line) are shown together with the energies of the $R(0)$ transition for CO in the gas phase ($2B$) and in ${}^4\text{He}$ droplets ($2B_{\text{eff}}$).

$$\epsilon(k_0) + \hbar^2 k_0^2 / 2M = \hbar \omega'. \quad (2.7)$$

It is evident from Eq. (2.6) that only the dipole coefficient $g_1(k)$ of the Legendre expansion of the helium-molecule pair distribution function $g(r, \cos \theta)$ contributes to the homogeneous rotational linewidth.

2. Applicability of the CBF/DMC bulk method for droplets

The CBF derivation of the molecular rotational spectra in bulk helium relied on the translational invariance of the ^4He environment, i.e., on the bulk limit,²⁹ while in a droplet there is no momentum conservation as a result of translational symmetry breaking. To our knowledge a quantitative expression for the self-energy in finite droplets has not yet been derived. This is a nontrivial task because of the translation symmetry breaking. Qualitatively, one can say that such an expression will involve a sum over discrete helium droplet modes rather than the integral over the continuous phonon-roton dispersion in the expression for bulk, Eq. (2.2). The finite droplet expression for $\Sigma_J(\omega)$ will furthermore involve a sum over the “particle-in-a-box” states, i.e., translational states of the molecule resulting from its confinement in the droplet, which can be represented by an effective potential.⁵⁷ We conjecture but cannot prove here, that these modifications will cause little change to the value of $\text{Re}\Sigma_J(\omega)$, and hence to the reduction of the B constant for a large droplet from its value in bulk helium. For example, replacing the k integral in Eq. (2.2) by a discrete, but dense sum amounts to calculating an integral by numerical quadrature. This is what is actually done for the bulk calculation, although the weights might be somewhat different. However, this argument is not applicable to the linewidth $\text{Im}\Sigma_J(\omega)$, Eq. (2.6). Formally, homogeneous broadening can arise only from the coupling of the molecular rotational modes J to a *continuum* of excitations, while coupling to discrete modes will lead to line splitting. Only if the discrete modes are sufficiently dense, can the expression (2.6) be considered to be a valid estimate of the linewidth. Here “sufficiently dense” means that the energy spacing of the discrete modes is much smaller than the linewidth Δ . A high density of states cannot derive from phonons nor from riplons (helium surface waves, see below), but is possible from the particle-in-a-box states of the molecule. In Ref. 57, coupling between rotational and particle-in-a-box states for HCN in a ^4He cluster of radius 30 Å was shown to lead to line broadening. With an effective potential⁵⁷ for CO in a cluster of radius 30 Å (and taking into account m splitting), and a Feynman phonon spectrum for a $^4\text{He}_{1000}$ cluster,¹⁸ we estimated that there are at least 5–10 combined discrete phonon and particle-in-box states within the experimental linewidth of 0.034 cm^{-1} in the energy range relevant for coupling to the $J=1$ rotation state of CO. Hence, despite the low density of phonon states in finite droplets, the high density of particle-in-a-box states can lead to the homogeneous line broadening seen in our IR spectrum.

A bulk calculation naturally excludes the effect of riplons on the molecular rotation. Due to their $\sim k^{3/2}$ dispersion, riplons have a higher density of states than long-wavelength phonons, on the order of three states per Kelvin for a cluster of radius 30 Å (still much less than the density

of states of particle-in-a-box states). On the other hand, the amplitude of ripplon excitations falls off exponentially with distance from the surface and they are therefore not expected to couple as efficiently as phonons to an embedded molecule.⁵⁷ Only a complete theory of linear rotors confined in a droplet can ultimately quantify the effect of riplons on molecule dynamics, i.e., on both the reduction in B and the linewidth.

3. Isotope effect on B_{eff}

Isotopic substitution has two effects on the coupling of the rotational motion of CO with ^4He : (a) the zero-point motion of heavier isotopomers is affected due to a change of the mass M and of the rotational constant B_0 ; and (b) the CO- ^4He interaction potential is slightly changed, mostly due to the shift Δz of the center of mass of the isotopomer. We shall take $^{12}\text{C } ^{16}\text{O}$ as the reference isotopomer, with index $i=1$. The potential $V(r, \cos \theta) \equiv V(x, y, z)$ is defined with respect to the centers of mass of CO and ^4He . A shift of the center of mass of CO corresponds to a shift of the potential in the opposite direction, $V(x, y, z + \Delta z)$. Table II lists the values Δz with respect to the center of mass of $^{12}\text{C } ^{16}\text{O}$ for all four isotopomers, obtained by assuming that the equilibrium distance between C and O itself is not affected by isotopic substitution. The two effects (a) and (b) can be considered independently in calculations, leading to a two-dimensional map $B_{\text{eff}} = B_{\text{eff}}(\Delta z, B_0)$. Hence the rotational constant in He droplets $B = B_{\text{eff}}$ should be regarded as a function of two variables, although experimentally we cannot distinguish between the influence of these. For small changes, we can expand the effective rotational constant of isotopomer i , $B_{\text{eff}}^{(i)}$, to first order in $\Delta z^{(i)}$ and in $\Delta B^{(i)} = B_0^{(i)} - B_0^{(1)}$:

$$B_{\text{eff}}^{(i)} = B_{\text{eff}}^{(1)} + \frac{\partial B_{\text{eff}}}{\partial B} \Delta B^{(i)} + \frac{\partial B_{\text{eff}}}{\partial \Delta z} \Delta z^{(i)}, \quad (2.8)$$

where $B_0^{(1)} = B_0$ and $B_{\text{eff}}^{(1)}$ are the reference ($^{12}\text{C } ^{16}\text{O}$) rotational constants in gas phase and in ^4He , respectively.

The response of the rotational spectrum to the small changes in B_0 and Δz (on the order of 10% from $^{12}\text{C } ^{16}\text{O}$ to $^{13}\text{C } ^{18}\text{O}$) necessary to evaluate the derivatives $\partial B_{\text{eff}} / \partial B$ and $\partial B_{\text{eff}} / \partial \Delta z$ is difficult to obtain by CBF/DMC and PICF. Correlated DMC or PIMC sampling^{60,61} has to be employed to reduce errors (from sampling) below the size of the changes of B_{eff} that are required. Consider first the derivative with respect to Δz . B_{eff} may be calculated as a function of a small potential difference resulting from the center of mass shift of Δz , and correlated sampling is thus straightforward to implement for the determination of $\partial B_{\text{eff}} / \partial \Delta z$. We determine $\partial B_{\text{eff}} / \partial \Delta z$ from the change of the $J=1$ rotational spectrum calculated with CBF, using the finite difference approximation for the differentiation

$$\frac{\partial B_{\text{eff}}}{\partial \Delta z} \approx \frac{B_{\text{eff}} - B_{\text{eff}}^{(1)}}{\Delta z}. \quad (2.9)$$

For that purpose, the pair distributions $g(r, \cos \theta)$ with $\Delta z = 0$ and a finite shift of $\Delta z = 0.1 \text{ Å}$, respectively, are determined with correlated sampling, expanded according to Eq.

(2.4), and substituted into the self-energy (2.2). From the resulting spectrum $S_j(\omega)$ Eq. (2.5), the respective values of B_{eff} and $B_{\text{eff}}^{(1)}$ are then obtained and inserted into Eq. (2.9).

We now consider the derivative with respect to B , $\partial B_{\text{eff}}/\partial B$. Unfortunately, correlated sampling is not feasible for sampling the response to small differences in the gas phase B values directly, since the latter derive from differences in rotational kinetic energy rather than from differences in potential energy. We therefore assume a simple linear scaling of B_{eff} with B_0 ;

$$\frac{\partial B_{\text{eff}}}{\partial B} \approx \frac{B_{\text{eff}}^{(1)}}{B_0^{(1)}}. \quad (2.10)$$

The first two terms in Eq. (2.8) can then be simplified to

$$B_{\text{eff}}^{(1)} + \frac{\partial B_{\text{eff}}}{\partial B} \Delta B^{(i)} = \frac{B_0^{(i)}}{B_0^{(1)}} B_{\text{eff}}^{(1)} = \frac{\mu^{(1)}}{\mu^{(i)}} B_{\text{eff}}^{(1)}, \quad (2.11)$$

where $\mu^{(i)}$ is the reduced mass of isotopomer i . Hence we get

$$B_{\text{eff}}^{(i)} = \frac{\mu^{(1)}}{\mu^{(i)}} B_{\text{eff}}^{(1)} + \frac{\partial B_{\text{eff}}}{\partial \Delta z} \Delta z^{(i)}. \quad (2.12)$$

III. RESULTS

A. Experiment

We produced He droplets at a stagnation pressure of $p_0 = 40$ bars, and temperature 20 K using a nozzle of $5 \mu\text{m}$ in diameter. Under these conditions the He droplets contain on average ~ 2600 He atoms.⁴¹ The peak mass of the mass spectrometer was adjusted to 28 amu and the diode laser was scanned between 2143.0 and 2145.5 cm^{-1} . In order to improve the signal to noise ratio, we reduced the resolution of the mass spectrometer so that several neighboring ions were transmitted. We tested the peak mass values 4, 8, 12, 16, and 28 amu and obtained the best signal to noise ratio using a mass of 12 amu.

The spectrum is shown in Fig. 3. We find a single line at $2145.412 \pm 0.001 \text{ cm}^{-1}$. The absorption intensity is given here in percent of the total beam depletion. Due to the

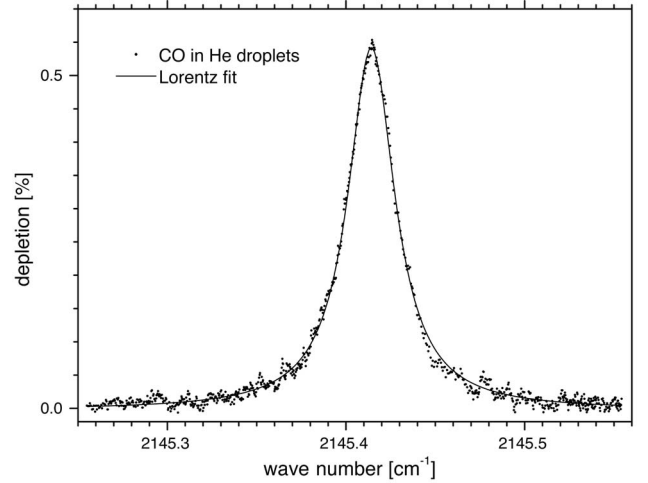


FIG. 3. The infrared spectrum of $^{12}\text{C } ^{16}\text{O}$ doped ^4He droplets with mean size $\bar{N} = 2600$. The solid line shows a Lorentzian fit to the experimental points.

very effective cooling in helium nanodroplets, only the $J=0, \nu_{\text{CO}}=0$ ground state is populated ($n_0/n \geq 99\%$). Therefore, the observed transition was assigned to the $R(0)\nu_{\text{CO}}=1 \leftarrow 0$ transition. The line is red shifted by 1.669 cm^{-1} from that of the free $^{12}\text{C } ^{16}\text{O}$ monomer in the gas phase.⁵³

The single spectral absorption line for all clusters of $\bar{N} \geq 2200$ can be fit very well with a Lorentzian line shape, indicating homogeneous line broadening. Multiple spectral scans were then fitted to obtain the average of the full widths at half maximum (FWHM) that are listed in Table I. We obtained a linewidth with negligible variation between values $0.033 \pm 0.002 \text{ cm}^{-1}$ for $^{13}\text{C } ^{16}\text{O}$ and $0.035 \pm 0.004 \text{ cm}^{-1}$ for $^{12}\text{C } ^{16}\text{O}$. It should be emphasized that the observed linewidth exceeds by far our experimental resolution ($\approx 0.003 \text{ cm}^{-1}$).

The beam depletion was measured at different pick up pressures, integrated after subtraction of a baseline, and normalized to the ion current. The dependence of the integrated absorption on the pick up pressure is shown in Fig. 4. The curve reveals a linear slope for small pick up pressures, con-

TABLE I. Experimental $R(0)$ frequencies, linewidths, B constants, and band origins of the isotopomers $^{12}\text{C } ^{16}\text{O}$, $^{13}\text{C } ^{16}\text{O}$, $^{12}\text{C } ^{18}\text{O}$, and $^{13}\text{C } ^{18}\text{O}$, in He droplets with $\bar{N} \sim 2600$ and in the gas phase (Ref. 53). The vibrational shifts are assumed identical for all four isotopomers. The standard deviations of the fits are 6% for B , and 0.15 cm^{-1} for the band origin. All units are in cm^{-1} .

	$^{12}\text{C } ^{16}\text{O}$	$^{13}\text{C } ^{16}\text{O}$	$^{12}\text{C } ^{18}\text{O}$	$^{13}\text{C } ^{18}\text{O}$
He droplets				
$R(0)$	2145.412	2098.142	2094.085	2045.602
Width	0.035 ± 0.004	0.033 ± 0.002	0.033 ± 0.001	0.034 ± 0.002
B	1.205	1.152	1.148	1.095
Band origin	2144.001	2095.837	2091.789	2043.412
Gas phase				
$R(0)$	2147.081	2099.710	2095.751	2047.154
B	1.913	1.830	1.823	1.739

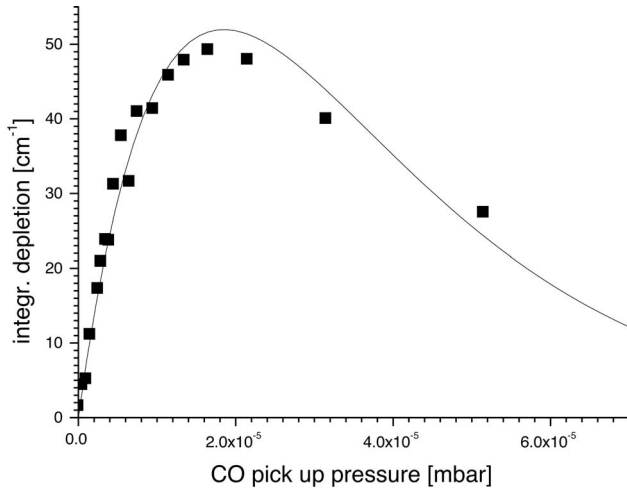


FIG. 4. Dependence of the integrated depletion signal of $^{12}\text{C } ^{16}\text{O}$ doped ^4He droplets with mean size $\bar{N}=2600$ on the pick-up pressure. The straight line is a fit using a Poisson function. The maximum for the monomer signal is achieved at $p_o=2 \times 10^{-5}$ mbar.

firming our assignment of the observed absorption line to the CO monomer. Furthermore, the dependence of the absorption intensity on the pick up pressure displays a maximum at 2×10^{-5} mbar, in agreement with the maximum signal for monomers derived from our mass spectrometric studies.

We also studied the influence of the average droplet size on the $\nu_{\text{CO}}=1 \leftarrow 0$ $R(0)$ absorption line, recording a set of spectra at different nozzle temperatures (Fig. 5). Although the spectra for the smaller droplets suffer from the reduced signal intensity, it is nevertheless evident from Fig. 5 that the center of the $R(0)$ line of $^{12}\text{C } ^{16}\text{O}$ shifts to larger wave numbers for droplets smaller than 2000 He atoms. Upon increasing the droplet sizes, no further shift is observed for $N \geq 2600$. We attribute the asymmetry in the line shape observed for smaller droplets to a size dependence of the transition frequency resulting from an underlying asymmetric droplet size distribution. Due to the limited signal, a more detailed investigation of the size dependence of the shift is not feasible at present.

Spectra of He droplets doped with isotopomers $^{13}\text{C } ^{18}\text{O}$, $^{13}\text{C } ^{16}\text{O}$, and $^{12}\text{C } ^{18}\text{O}$ were recorded in the same manner. These spectra are displayed in Fig. 6 for droplets with average size $\bar{N}=2600$. All spectral lines are found to fit perfectly to a Lorentzian line shape. The line frequencies and width values obtained from averaging over multiple scans are presented in Table I. The beam depletion spectra are shown in Fig. 6. The intensity differs between the individual spectra. This is attributed to differences in the output power of our laser diodes or to a variation of the residual gas pressure that enhances depletion.

The measurement of the $R(0)$ transition of several isotopomers allowed us to extract both the rotational constant in He droplets, B_{eff} , and the shift α of the band origin with respect to the gas phase value ν .⁵³ If we assume an identical magnitude of the shift α for all isotopomers, and that the difference between the B_0 constants of all isotopomers is

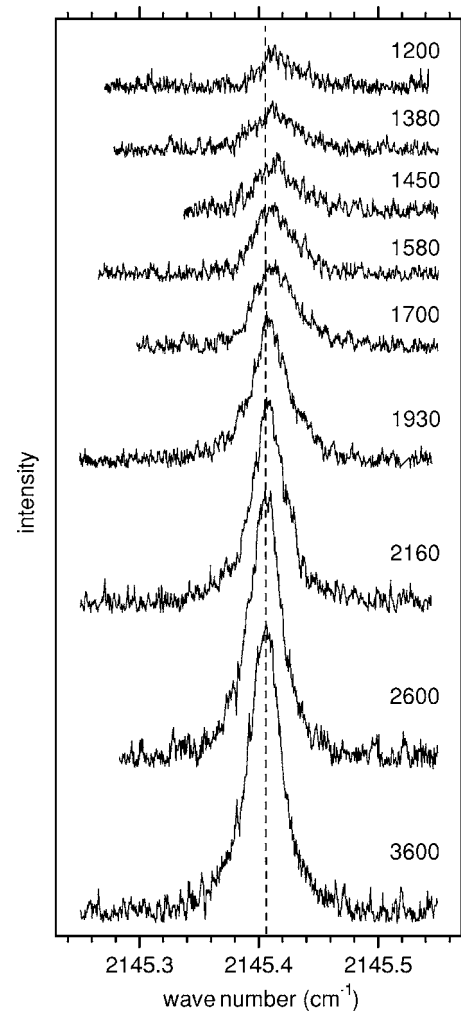


FIG. 5. Absorption spectra of $^{12}\text{C } ^{16}\text{O}$ in He droplets for different average droplet sizes ($\bar{N}=1200\text{--}3600$). The line shape and the peak position remain unchanged for droplet sizes above $\bar{N}=2200$. Smaller droplets reveal a blue shift that becomes stronger with decreasing size and an increasingly asymmetric line shape. The dashed line visualizes the shift.

given by the ratio between their reduced masses, then we can express the measured $R(0)$ frequency ω_i of isotopomer i as a function of $\nu^{(i)}$, α , and $\mu^{(1)}/\mu^{(i)}$. From Eq. (2.12) we get

$$\omega^{(i)} = \nu^{(i)} + \alpha + 2 \frac{\mu^{(1)}}{\mu^{(i)}} B_{\text{eff}}^{(1)} + 2 \Delta_z B_{\text{eff}}^{(i)}. \quad (3.1)$$

The last term $2 \Delta_z B_{\text{eff}}^{(i)} = 2(\partial B_{\text{eff}}/\partial \Delta z) \Delta z^{(i)}$ is induced by the change of the center of mass in the intermolecular potential. This term has been calculated as described in Sec. II B 3 and is listed in Table II for all isotopomers.

We can then deduce α and the rotational constant $B_{\text{eff}}^{(1)}$ of the reference isotopomer $^{12}\text{C } ^{16}\text{O}$ from a linear fit on plotting $(\omega^{(i)} - \nu^{(i)} - 2 \Delta_z B_{\text{eff}}^{(i)})$ against $2 \mu^{(1)}/\mu^{(i)}$. This plot is shown in Fig. 7 (squares), together with the linear fit. The resulting effective rotational constant $B_{\text{eff}}^{(1)}$ of $^{12}\text{C } ^{16}\text{O}$ corresponds to $63 \pm 2\%$ of the corresponding gas phase value⁵³ and the band

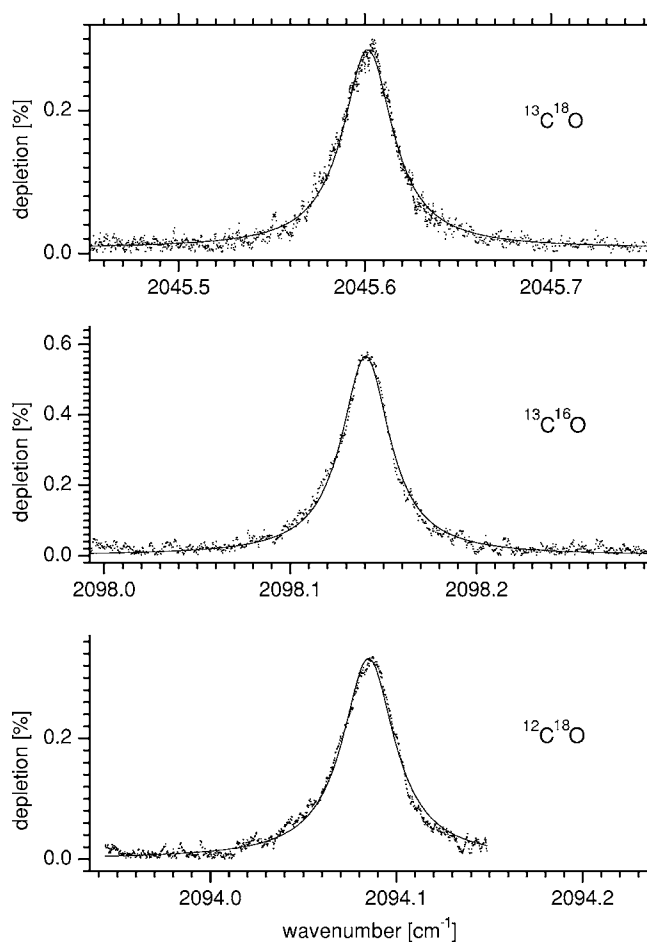


FIG. 6. Spectra of $^{13}\text{C}^{18}\text{O}$, $^{13}\text{C}^{16}\text{O}$, and $^{12}\text{C}^{18}\text{O}$ doped He droplets with mean size $\bar{N}=2600$ (points). All spectra can be fitted to Lorentzian functions (solid lines). The resulting linewidths are given in Table I. The intensity is given here as a percentage of the beam depletion.

origin is shifted by $\alpha = -0.254 \pm 0.07 \text{ cm}^{-1}$ from its gas phase value.

We note that if the correction term $2\Delta_z B_{\text{eff}}^{(i)}$ is neglected, a plot of $(\omega^{(i)} - \nu^{(i)})$ would result in a reduction in $B_{\text{eff}}^{(1)}$ of 68%. While this reduction is similar to that extracted from $(\omega^{(i)} - \nu^{(i)} - 2\Delta_z B_{\text{eff}}^{(i)})$, the corresponding data points would deviate much more strongly from a linear slope, as is evident in Fig. 7 where these points are shown as circles. The quality of the fit is improved significantly by the correction term which emphasizes the relevance of the isotope-induced change of the intermolecular potential and the corresponding change in rotational energy. We have assumed an identical “matrix shift

TABLE II. Center of mass shift, Δz and correction of the effective rotational constant, $2\Delta_z B_{\text{eff}}$, of the four isotopomers with respect to the reference species $^{12}\text{C}^{16}\text{O}$ [see Eq. (2.8)].

	$^{12}\text{C}^{16}\text{O}$	$^{13}\text{C}^{16}\text{O}$	$^{12}\text{C}^{18}\text{O}$	$^{13}\text{C}^{18}\text{O}$
Δz	0.0 Å	-0.0222 Å	0.0322 Å	0.0104 Å
$2\Delta_z B_{\text{eff}}$	0.0 cm^{-1}	0.034 cm^{-1}	-0.050 cm^{-1}	-0.016 cm^{-1}

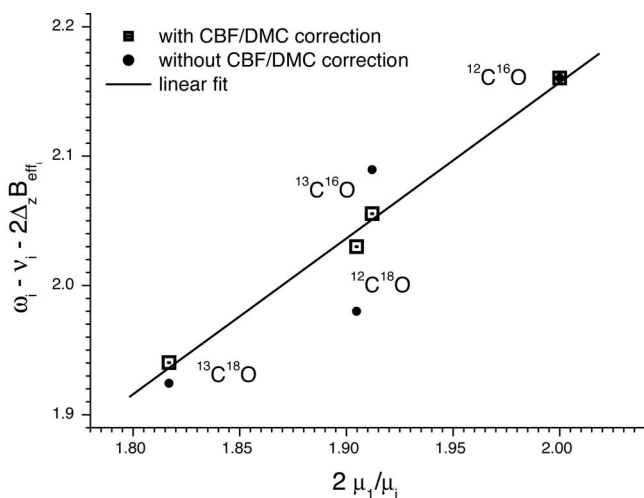


FIG. 7. Rotational energies of CO isotopomers plotted versus the ratios of the reduced masses (squares). μ_i is the reduced mass of the isotopomer i , with $i=1$ denoting the reference $^{12}\text{C}^{16}\text{O}$ species. ω_i is the measured frequency in He droplets, ν_i the band origin in the gas phase, and $2\Delta_z B_{\text{eff}}$ the isotope-induced correction (see text). A linear fit allows the magnitude of the shift of the band origin α and the rotational constant B_{eff} of $^{12}\text{C}^{16}\text{O}$ in He droplets to be determined, provided that α is identical for all isotopomers and that the difference in the rotational constants between all isotopomers is controlled by their respective reduced masses and isotope-induced correction only (see text). For comparison, we also show the rotational energies without the correction $2\Delta_z B_{\text{eff}}$ (large dots). The isotope-induced shift of the intermolecular potentials $2\Delta_z B_{\text{eff}}$ is opposite for $^{13}\text{C}^{16}\text{O}$ and $^{12}\text{C}^{18}\text{O}$ and is significant for the quality of the fit. All units in cm^{-1} .

“ α ” for all four isotopomers since introducing further parameters would not lead to a better fit result. A mass scaling of these parameters would have a negligible influence on the final result. Even a 10% deviation, which corresponds to shifts in the order of 0.025 cm^{-1} that can hardly be seen in Fig. 7, would lead only to minor changes in B_{eff} . As will be discussed in Sec. IV, the fit supports strongly the validity of our model and shows its significance for the prediction of accurate rotational constants in He droplets.

B. CBF and PICF calculations

The rotational spectrum of $^{12}\text{C}^{16}\text{O}$ was calculated in bulk helium using the CBF/DMC method. From the calculated $J=1$ rotational energy, we derive an effective rotational constant $B_{\text{eff}}^{(1)}$ which is reduced to $69 \pm 2\%$ of the gas phase value $B_0^{(1)}$. This is slightly higher than the experimentally determined value of 63%. Such a deviation is similar to that seen previously with CBF/DMC calculations for HCN (Ref. 29) and HCCH.³⁰ After correcting for the finite size effects of the DMC simulation, we obtain a FWHM linewidth of $2\Delta = 0.018 \pm 0.002 \text{ cm}^{-1}$. This is about one-half of the measured linewidth. In Sec. IV we discuss these results for the spectra $S_J(\omega)$ and explain its main features—the large reduction of B_{eff} and large linewidth—in terms of the CBF theory.

To assess the effect of cluster size on rotational constant we also performed a PIMC simulation for a cluster of $64 \text{ }^4\text{He}$

TABLE III. Rotational constants B_0 (in the gas phase) and B_{eff} (in He droplets), rotational excess energies (the energy which is released by rotational relaxation), and linewidths of several light rotors in He droplets. B' and B'' refer to different B constants of the upper and lower vibrational levels. All units are in cm^{-1} .

Molecule	B_0	B_{eff}	Rotational excess energy	FWHM linewidth	Transition
HF	19.787	19.48	38.96	0.43	R(0) (Ref. 84)
HF	19.787	19.48	0	0.007	Q(0) (Ref. 84)
NH ₃	9.96	7.5	15	3.2	R(0 ₀ ⁻) (Ref. 96)
CH ₄	5.256 (B'')	5.012 (B'')	0	0.25	R(0) (Ref. 85)
	5.196 (B')	4.932 (B')			
CH ₄	5.256 (B'')	5.012 (B'')	19.305	1.1	R(1) (Ref. 85)
	5.196 (B')	4.932 (B')			
¹² C ¹⁶ O	1.931	1.205	2.410	0.035	R(0) this work
HCN	1.478	1.175	2.350	0.0067	R(0) (Ref. 27)
¹³ C ¹⁶ O	1.830	1.152	2.284	0.033	R(0) this work
¹² C ¹⁸ O	1.823	1.148	2.276	0.033	R(0) this work
¹³ C ¹⁸ O	1.739	1.095	2.170	0.034	R(0) this work
¹² C ₂ H ₂	1.177 (B''), 1.172 (B')	1.04	0	0.043	R(0) (Ref. 21)
¹² C ₂ H ₂	1.177 (B''), 1.172 (B')	1.04	3.54	0.145	R(1) (Ref. 21)

atoms, containing approximately two full solvation shells of helium. This calculation yielded a reduction of the B constant to 77 ± 1 % of $B_0^{(1)}$. Thus the B constant calculated for these intermediate size clusters is closer to the gas phase value than those calculated by CBF/DMC for bulk and found experimentally in large droplets.

The specific influence of isotopic substitution on the change of the constant B_{eff} has been evaluated in Sec. II B 3. The changes of the center of mass in the interaction potential and the resulting energy shifts are given in Table II.

IV. DISCUSSION

A. Shift of $R(0)$ frequency

As described in Sec. III A, the single line measured in the infrared spectrum is shifted from the gas phase value by a combination of the vibrational shift for $\nu_{\text{CO}}=1 \leftarrow 0$ which moves the band origin, and a rotational shift for the $R(0)$ transition that results from a reduction in the effective B value. As described above, the measurements for four isotopomers here allowed us to extract both of these contributions, yielding a vibrational shift value of $\alpha = -0.254 \pm 0.07 \text{ cm}^{-1}$ (assumed to be isotopomer independent) and the reduced B values $B_{\text{eff}}^{(i)}$ listed in Table III. For the normal ¹²C ¹⁶O isotope, we extract a value of $B_{\text{eff}}^{(1)}$ reduced to 63% of the gas phase value. Figure 8 shows the measured $R(0)$ frequencies for the three CO isotopomers that have also been studied in small clusters by Tang and McKellar,^{31,32} together with the two sets of size-dependent $R(0)$ transitions observed in those measurements. At the smallest N values, those experiments showed two transitions, designated a -type and b -type in Ref. 31 by analogy with the known spectrum for $N=1$. Above $N=11$, except for an anomalous splitting at $N=15$, only a single transition was seen. In that work the vibrational and rotational contributions to the frequency

could not be separated, but we can nevertheless compare the absolute position of the spectral peak. By extrapolation, Tang and McKellar predicted a frequency of 2145.7 cm^{-1} for the normal isotope in large droplets, which is 0.288 cm^{-1} higher than our experimentally determined value of 2145.412 cm^{-1} (see bottom panel of Fig. 8).

The vibrational shift, in particular, the blue shift associated with the surrounding He cluster, is difficult to predict. The size dependence of vibrational shifts has been analyzed for SF₆ in Refs. 62 and 63 where it is found that the main contribution to the shift derives from the first solvation shell. The long range molecule-solvent atoms interaction amounts to $-C_6/r^6$ and may be treated as pairwise additive.⁶⁴ In many cases a red shift follows from an increased C_6 value upon vibrational excitation. ΔC_6 is the difference between the C_6 values in the $\nu=0$ and $\nu=1$ states. Three factors contribute to ΔC_6 . (i) The normalized difference $\Delta \gamma_{\text{pol}} / \gamma_{\text{pol}} C_6$ between the polarizability of the dopant molecule in the two states $\nu=0$ and $\nu=1$. (ii) The instantaneous transition dipole-induced dipole interaction.⁶⁵ (iii) The difference of the static dipole moment of the dopant molecule between the $\nu=0$ and $\nu=1$ states. The overall shift can be expressed as

$$\Delta \nu = -4\pi \Delta C_6 \int \frac{\rho(r)}{r^4} dr, \quad (4.1)$$

when the dopant molecule is assumed to reside in the center of a spherical cluster. We can make a rough estimate of the change in vibrational shift on going from a cluster size corresponding to only one solvation shell to the bulk system by making use of the excluded volume model:⁶⁶

$$\Delta \nu(N) = \left(\frac{4}{3} \pi \rho_0 \right)^2 \frac{\Delta C_6}{N}. \quad (4.2)$$

Here ρ_0 is the bulk density of helium, which is taken as 0.0218 \AA^{-3} . Calculation of absolute shifts is difficult in gen-

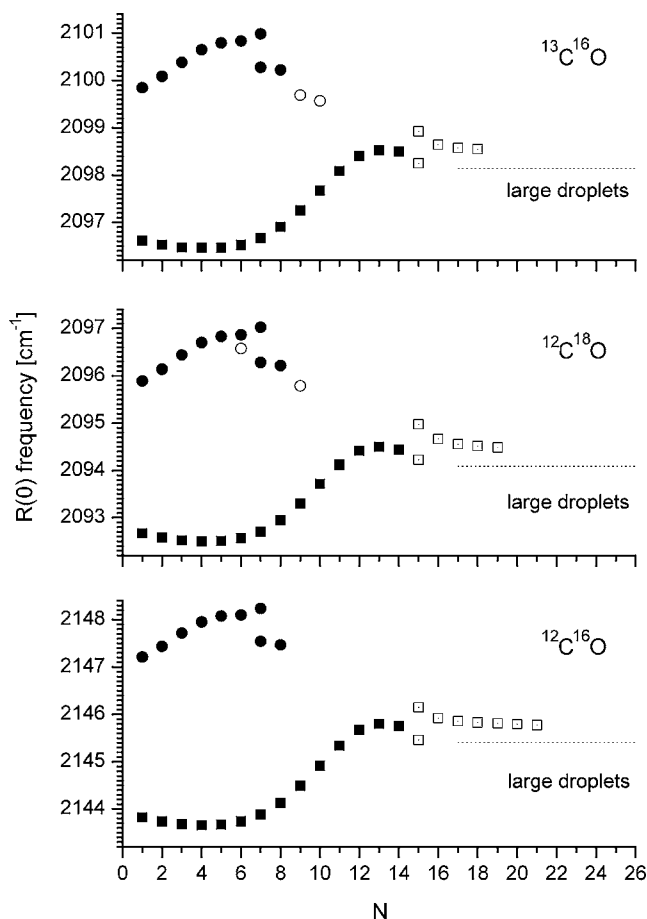


FIG. 8. Cluster size dependence of the a -type and b -type $R(0)$ transitions for $^{12}\text{C }^{16}\text{O}$, $^{13}\text{C }^{16}\text{O}$, and $^{12}\text{C }^{18}\text{O}$ in small helium clusters (Refs 31 and 32) is shown together with the corresponding $R(0)$ transition frequencies in large droplets measured in this work. N is the number of He atoms. The solid squares refer to reliable assignments, the hollow squares to tentative assignments of a -type frequencies, respectively, from the work of Tang and McKellar (Refs. 31 and 32). The b -type frequencies are indicated by solid circles, with hollow circles similarly indicating tentative assignments. The horizontal dotted lines represent the transition frequency in large droplets reported in this work.

eral, because the values depend sensitively on the He density distribution around the dopant molecule. Therefore, we merely compare here the change in shift between a small cluster of $N \sim 20$, and the large droplets with $N=2600$ that are accessible in the present experiments. The difference between the shift for two different droplet sizes can be estimated from evaluation of the upper limit of the integral in Eq (4.1) for different values of the cluster radius, R . Using the transition dipole moment value of Ref. 67, ΔC_6 from Ref. 68, and C_6 from Ref. 69, we find that the overall change in vibrational shift between $N \sim 20$ and $N=2600$ is approximately 0.17 cm^{-1} for CO. This value should be considered as an upper bound on the difference, since we neglect the contribution of any blue shift as well as the effects of higher order polarizabilities (C_8 or C_{10}) which are often important at small internuclear distances.

We have also calculated the vibrational shift α in bulk helium as the difference between averages of the vibra-

tionally averaged CO-He interaction potentials in the ground and first excited CO vibrational states:

$$\alpha \approx 2\pi\rho \int dr r^2 d(\cos \theta) g(r, \cos \theta) \times [V(r, \cos \theta) - V_{11}(r, \cos \theta)]. \quad (4.3)$$

Here V_{11} describes the CO-helium potential of the $\nu=1$ vibrational state³³ and $V(r, \cos \theta) \equiv V_{00}$ is the corresponding potential for the $\nu=0$ vibrational state. The average is taken over the two-particle density derived from the CO-helium pair distribution $g(r, \cos \theta)$ obtained from our DMC simulation of CO in bulk ^4He for $\nu=0$. This vibrationally adiabatic calculation yields a value $\alpha = -0.84 \text{ cm}^{-1}$, which is larger than the experimental value for α that is obtained by fitting Eq. (3.1). However, as was already noted in Ref. 33 in calculations of vibrational shifts for $N=1$, these potentials V_{11} and V_{00} do overestimate the magnitude of the red shift. A similar overestimate is expected for the present case so our order of magnitude agreement is quite adequate, however it does not allow us to yield a quantitative prediction of the vibrational shift.

B. Reduction of rotational constant

For all molecules solvated in He droplets to date, a reduction of the B constant has been reported.⁷⁰ Depending on the moment of inertia there are two different regimes. For heavy, slow rotors with gas phase rotational constants of $\leq 0.25 \text{ cm}^{-1}$ an average reduction to about one-third of the gas phase value is found, while for lighter, fast rotors there is much less relative reduction of B . For the heavier molecules the reduction has been assigned to the fact that some fraction of the ^4He density in the first solvation shell (for larger complexes, also in the second solvation shell⁷¹) can adiabatically follow the rotational motion and thereby contribute to the moment of inertia.¹⁵ For the lighter molecules, the CBF calculation suggests a mechanism where the molecular rotation couples to elementary excitations which are extended over and beyond the local solvation region of the ^4He droplet. In both cases, the coupling of molecules and ^4He atoms depends on the speed of rotation,⁷² i.e., the rotational constant, and on the shape and the depth of the intermolecular potential, particularly on the anisotropy. The importance of the potential is highlighted by comparison of CO with HCN. HCN has a gas phase rotational constant of $B_0 = 1.478 \text{ cm}^{-1}$ and is thus *slower* than CO ($B_0 = 1.922 \text{ cm}^{-1}$). Nevertheless, the relative B reduction for HCN amounts to $B_{\text{eff}}/B_0 = 79\%$,²⁷ while for CO we find here a stronger reduction of $B_{\text{eff}}/B_0 = 63\%$. We will show now that these differences in the reduction of B can be attributed to the higher degree of anisotropy of the intermolecular potential for CO, which increases the coupling strength between CO and helium, resulting in a larger cloud of virtual phonons dragged by the rotating CO.

1. Anisotropy

The interaction potential $V(r, \cos \theta)$ between CO and ^4He (Ref. 33) is shown in Fig. 9, together with the corresponding potentials for the molecules HCN (Ref. 73) and HCCH.⁷⁴

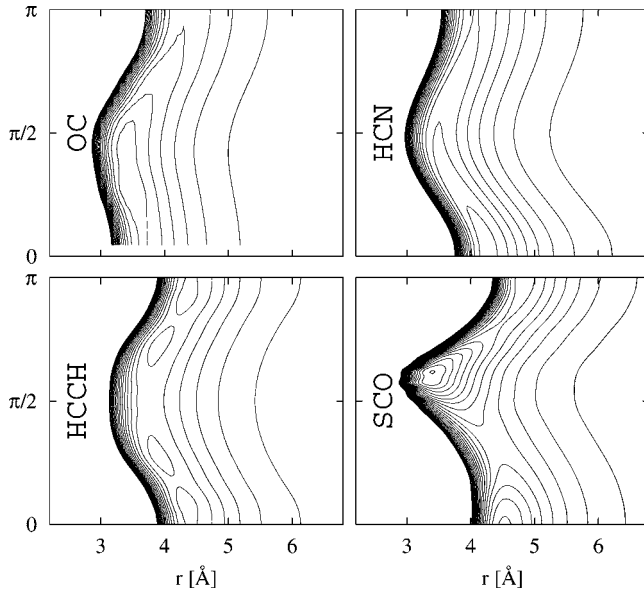


FIG. 9. Comparison of helium interaction potentials for CO, HCN, and acetylene (HCCH). Also shown for comparison is the potential of the much heavier OCS molecule with helium. $r=|\mathbf{r}|$ where \mathbf{r} is the position of the ^4He atom in the center of mass frame of CO. θ is the angle between the CO symmetry axis and \mathbf{r} . The orientation of the molecule is defined by the atomic symbols. Contour lines are shown in steps of 5 K.

The corresponding potential for the heavier rotor OCS (Ref. 75) is also shown for comparison. The most noticeable difference in the interaction potentials of the three light molecules HCN, HCCH, and CO with ^4He is the degree of anisotropy. In comparison to HCN and to HCCH, CO shows a marked asymmetry with respect to the plane perpendicular to the molecule axis. While the HCCH potential obviously is exactly symmetric and the HCN potential is only slightly asymmetric, the CO- ^4He potential is much more egg-shaped. This leads to a larger asymmetry of the CO- ^4He pair distribution function $g(r, \cos \theta)$. Figure 10 shows the anisotropic part of $g(r, \cos \theta)$ for CO, obtained by subtracting the rota-

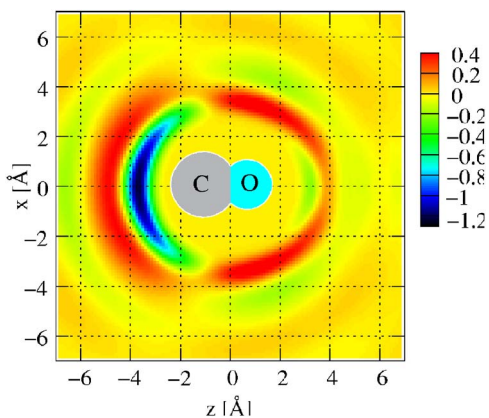


FIG. 10. (Color online) The anisotropic component of the CO-helium pair distribution function $g(r, \cos \theta)$, i.e., the pair distribution function *without* the spherical contribution in a Legendre expansion, $g(r, \cos \theta) - g_0(r)$.

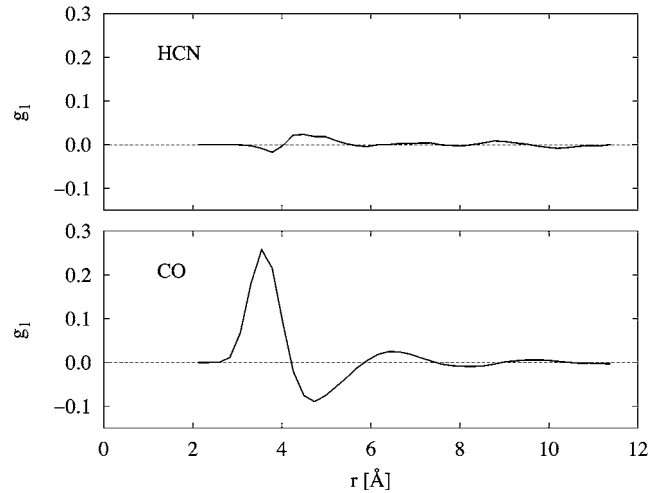


FIG. 11. Comparison of the $\ell=1$ components $g_1(r)$ of the Legendre expansion of the pair distribution function $g(r, \cos \theta)$ between helium and HCN and CO, respectively, as obtained from DMC simulation in bulk helium. Note that for HCCH, $g_1(r)$ vanishes due to symmetry (Ref. 30).

tionally averaged pair distribution $g(r)$ from $g(r, \cos \theta)$. This is further decomposed in Fig. 11, which shows the “dipole,” $\ell=1$, component $g_\ell(r)$ of the Legendre expansion of $g(r, \cos \theta)$ for HCN and for CO (this term is identically zero for HCCH as a result of the molecular symmetry). From this it is evident that the contributions from $g_\ell(k)$ for $\ell=1$ (and, in fact, more generally for odd ℓ) to the self-energy $\Sigma_f(\omega)$, Eq. (2.2), and hence to the spectrum $S_f(\omega)$ increase substantially from HCCH to HCN to CO. As a result, the decrease of the effective rotational constant B_{eff} is largest for CO and smallest for HCCH, with HCN being an intermediate case. The CBF spectrum for $J=1$ yields a relative reduction of $B_{\text{eff}}/B_0=0.69\pm 0.02$ for $^{12}\text{C}^{16}\text{O}$, which is close to the value 0.63 that is extracted from the experiment. Closer examination of the self-energy shows that about *half* of this reduction of B_{eff} comes from the $\ell=0$ term in Eq. (2.3). Due to the selection rules for $J=1$, which are mediated by $\tilde{L}(J, \ell', \ell)$, only the dipole coefficient $g_{\ell'=1}(k)$ contributes to this $\ell=0$ term. Therefore at least half of the reduction of B_{eff} can be directly assigned to the dipole component of the pair distribution, and hence to the pronounced egg-shaped nature of the CO- ^4He potential. The much greater value of this dipole component for CO than for HCN and HCCH thus provides a quantitative explanation of the stronger reduction of B_{eff} for CO, in this series of light molecules with similar effective rotational constants.

2. Size effect

In Fig. 12, the self-energy density $\sigma_1(\omega, p)$ at the transition energy $\omega=\omega'$ shows that the contributions to $\Sigma_1(\omega')$ come from a wide range of wave vectors k , spanning wave vectors of phonons, maxons, and rotons. Note that at $k_0=0.2 \text{ \AA}^{-1}$, $\sigma_1(\omega', k)$ diverges for CO because the energy denominator vanishes, which is responsible for the finite linewidth. The associated divergence for HCN is much

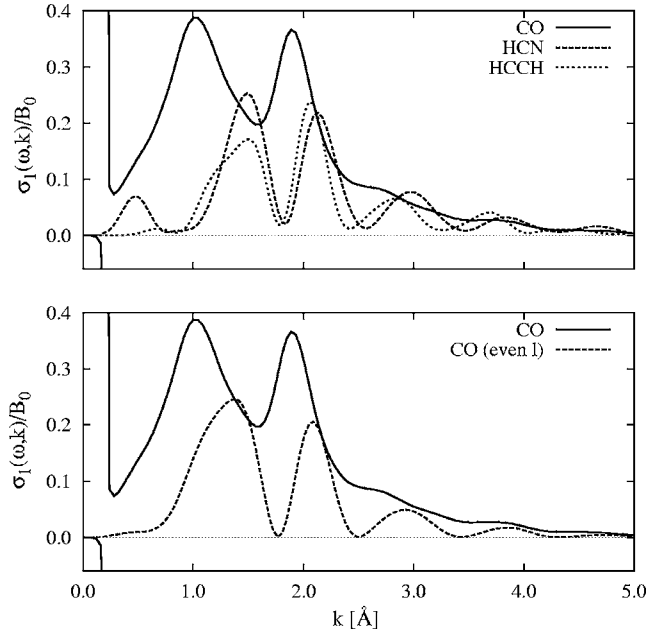


FIG. 12. The CBF/DMC self-energy momentum density $\sigma_1(\omega, k)$ (scaled by the gas phase value of B) is shown for the $J=0 \rightarrow 1$ transition of CO, HCN, and HCCH (upper panel). Note that, for HCCH, this transition is only allowed in the rovibrational spectrum. The lower panel compares $\sigma_1(\omega, k)$ of CO with that for a hypothetical symmetric CO molecule, for which only even ℓ components of the pair density distribution are retained in calculation of $\sigma_1(k)$.

smaller and not resolved in Fig. 12, while for HCCH the energy denominator does not diverge due to HCCH's symmetry (for HCCH, the $J=0 \rightarrow 1$ transition is not allowed in the rotational spectrum, but is allowed in the rovibrational spectrum). Clearly, wave vectors on the order of the roton wave vectors of $k \approx 2 \text{ \AA}^{-1}$ contribute prominently, as do wave vectors corresponding to the maxon regime. However, we also see that wave vectors below $k=1 \text{ \AA}^{-1}$, corresponding to wavelengths $\lambda > 6 \text{ \AA}$, cannot be neglected for CO, while for HCN small wave vectors contribute less, and for HCCH almost nothing. In the lower panel, we compare $\sigma_1(\omega, k)$ of CO with that for a hypothetical *symmetric* CO for which all odd ℓ' values are omitted in Eq. (2.3). For the hypothetical symmetric CO, $\sigma_1(\omega, k)$ is very similar to that of HCCH, showing that coupling between molecule and long-wavelength phonons can be directly correlated to the asymmetry of the molecule-helium interaction potential.

Small clusters of one or two solvation shells cannot support long-wavelength phonons. Hence, if the associated low wave vector range of $\sigma_1(\omega', k)$ (Fig. 12) is excluded from the integration in Eq. (2.2), the magnitude of the self-energy Σ_1 is reduced, and B_{eff} will be closer to the gas phase value. This is exactly what we observe in our PICF simulation of the rotational spectrum of CO in a cluster of $N=64$ ^4He atoms (approximately two solvation layers), which reveals a relative reduction of $B_{\text{eff}}/B_0=77\%$. This is considerably larger than both our CBF value for bulk (69%), and our experimental value for $\bar{N}=2600$ (63%). It is also consistent with the experimental results for small clusters^{31,32}

(see Sec. IV A). We propose therefore that the observed red shift of the $R(0)$ line from clusters of $N \approx 20$ to $N \approx 2200$ is partly due to a slow reduction of B_{eff} with size N towards a saturation value at $N=\infty$, in addition to some change in value of the vibrational shift. The CBF analysis confirms that this saturation is expected to be slower for asymmetric molecules like CO.

Figure 13 shows the rotational excitation energies resulting from B_{eff}/B_0 for CO over the entire range of N accessible to either experiment or theory, and compares with the corresponding size dependence for several other small linear molecules.

3. Isotope effect

The isotope effect on the reduction of the rotational constant in the large clusters that is measured here can be readily explained by the changes in the intermolecular potential that are induced by the isotopic substitution, as described in Sec. II B 3. The main potential change will originate from the shift of the center of mass of the isotope, which affects the degree of asymmetry of the potential. The resulting corrections to B_{eff} obtained upon changing the center of mass [i.e., the third term in Eq. (2.8)], are summarized in Table II, where the reference is taken as $^{12}\text{C } ^{16}\text{O}$. The nonlinear dependence of the isotope-dependent difference $(\omega^{(i)} - \nu^{(i)})$ on the mass ratio $\mu^{(1)}/\mu^{(i)}$ when the correction $2\Delta_z B_{\text{eff}}^{(i)}$ is neglected (see Fig. 7) can thus be attributed to this isotopic potential shift. This is particularly evident for the isotopomers $^{12}\text{C } ^{18}\text{O}$ and $^{13}\text{C } ^{16}\text{O}$. The agreement between experiment and theory is excellent. We emphasize that the nonlinear behavior of the isotope correction measured here demonstrates that the rotational spectra of molecules in ^4He and the derived quantities such as B_{eff} , should not be regarded as a function of the gas phase rotational constants or reduced masses alone, but also of the molecule-helium interaction.

C. Line broadening

Various sources of line broadening in He droplets are discussed in the literature. Inhomogeneous broadening has been frequently observed for smaller droplet sizes^{23,63,76-80} and is evident here for the smaller droplets with $\bar{N} \leq 2200$. This effect derives from the droplet size distribution in the beam, which is superimposed on any underlying size dependence of the line frequencies. Any asymmetry of the droplet size distribution therefore results in asymmetric line profiles.⁸⁰ Inhomogeneous line broadening can also originate from anisotropic forces in the droplet potential that may arise from a displacement of the molecule from the droplet center and the finite size of the droplets.^{57,81} The effect of inhomogeneous broadening for a single cluster size has been experimentally verified by measuring the dependence of the absorption signal on the intensity of a microwave field.⁷⁸⁻⁸⁰

In Fig. 5 we observe an increasing linewidth and asymmetry as the average droplet size decreases below $\bar{N} \sim 2200$, consistent with inhomogeneous broadening due to a finite droplet size distribution. However, above this average drop-

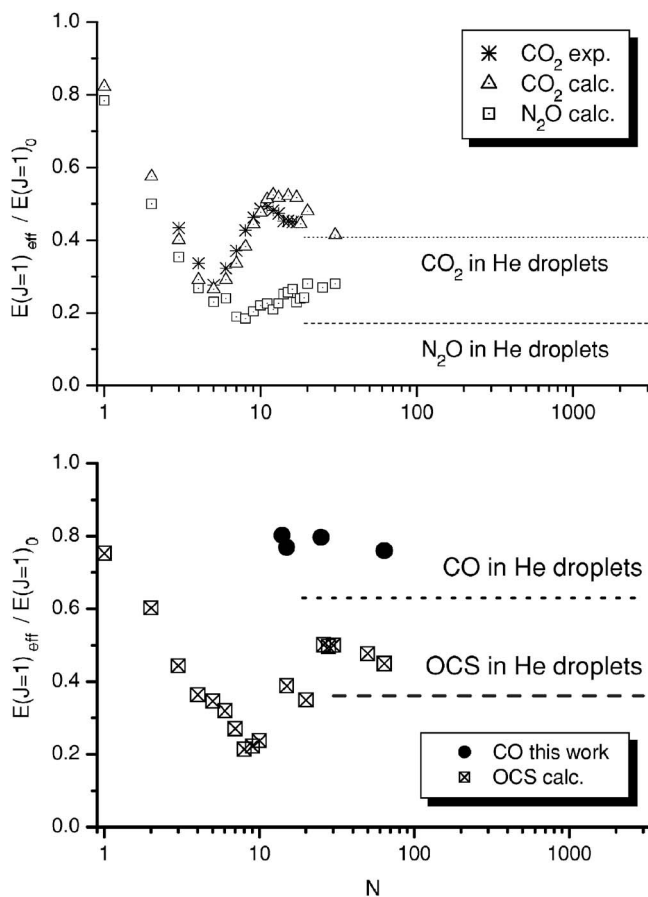


FIG. 13. The renormalization of the rotational levels in He droplets is shown as a function of the cluster size N for CO from this work and compared with experimental and theoretical values for several different molecules. We show $E(J=1)/E(J=1)_0$ instead of B_{eff}/B_0 , since experimental values of B are sometimes but not always fit together with the distortion constant D , which modifies the fit values. Experiment: CO_2 values from Refs. 93 and 94, N_2O values from Refs. 92 and 94, OCS values from Refs. 90 and 91. Theory: CO_2 from Refs. 89 and 95, N_2O from Refs. 87 and 95, OCS from Refs. 38, 86, 88, and 95.

let size the line shape is symmetric and well fit by a Lorentzian with a constant linewidth. Homogeneous broadening derives from the finite lifetime of the excited state and gives rise to Lorentzian-shaped absorption lines. Hence we see a gradual transition from inhomogeneously broadened spectral lines at the smaller values of \bar{N} to homogeneous broadening for values above a typical size of $\bar{N} \sim 2200$. Taking the almost perfect fit of the Lorentzian line-shape profile for droplets larger than the critical size regime, e.g., for $N=2600$, we can extract a lifetime of 1.56×10^{-10} s.

Assuming homogeneous broadening for the $R(0)$ line above $\bar{N} \sim 2200$, this lifetime can be attributed to rotational or vibrational relaxation. Lorentzian line shapes have been observed in the spectra of both SF_6 (Ref. 40) and H_2O ,⁸² where they were associated with limited vibrational lifetimes in both cases. Polyatomic molecules can have vibrational modes in resonance with combinations of lower energy vibrational modes. The broad linewidths of acetylene²¹ and

HCN dimers have been attributed to enhanced vibrational relaxation proceeding via combination bands.⁸³ As noted earlier, helium droplets doped with HF and with HF-rare-gas complexes reveal unusually long vibrational lifetimes, indicating that vibrational relaxation is inefficient and takes place on a time scale of msec,^{46,50,84} possibly even exceeding the time of flight. For the rare-gas complexes a gradual increase of the relaxation rate with the mass of the rare-gas species is observed, consistent with an increasing density of states for the intermolecular modes.⁵⁰ Because CO has only a single vibrational mode 2150 cm^{-1} above the ground state, and because CO has also been confirmed to show extremely long vibrational-translational lifetimes in liquid nitrogen and argon,⁴³⁻⁴⁵ we can exclude vibrational relaxation as an efficient relaxation mechanism for this molecule in helium. Consequently, it appears that the homogeneous lifetimes must reflect rotational relaxation times.

Rotational relaxation has been identified as the dominating relaxation channel for HF (Ref. 84) and for the $R(1)$ line of CH_4 .⁸⁵ High frequency modulation of the amplitude of a microwave field may also provide an upper limit of the rotational relaxation time, as has been shown for HCCCN (2–20 ns).⁷⁸ This lifetime has been attributed to rotational-riplon coupling.⁷⁹

For CO we postulate that the coupling to collective excitations of the appropriate energy, in particular, rotons and phonons, only show up in large droplets above a specific size. Consequently, this relaxation mechanism will be absent in smaller clusters. This is illustrated explicitly in Fig. 14, where we compare the line profile of our spectrum for $\bar{N} \sim 2600$ with that recently measured for CO in the very small $^4\text{He}_N$ clusters ($N \leq 20$).^{31,32} Whereas for the latter the lines are very sharp (100 MHz) and within the laser linewidth, the line for $\bar{N} \sim 2600$ is broadened. This lack of homogeneous broadening at small sizes indicates a lack of excitations in the helium layer having the appropriate energy to couple efficiently to the CO $J=1$ rotation.

In our bulk CBF/DMC calculation, in order to fulfill energy and momentum conservation, rotational relaxation should be accompanied by both the creation of a long-wavelength phonon ($\lambda = 2\pi/k_0 \sim 30 \text{ \AA}$) and simultaneous excitation of translation of the molecule. Clusters of only $N \sim 20$ atoms are too small to support such a phonon. [The wave vectors of the excited phonon, $k_0 = 0.20 \text{ \AA}^{-1}$, are determined from Eq. (2.7).] In addition, small clusters do not support a sufficiently dense spectrum of particle-in-a-box states. In contrast, the higher combined density of states in large droplets provides a quasicontinuum of final states which can result in homogeneous broadening, leading to the observed Lorentz-shaped line at large enough size.

We have calculated the homogeneous linewidth of the $J=1$ state from CBF theory, using Eq. (2.6), for CO in bulk helium. These calculations result in a FWHM value of $2\Delta = 0.018 \pm 0.002 \text{ cm}^{-1}$, accounting for about half of our measured FWHM linewidth of 0.034 cm^{-1} . However, there

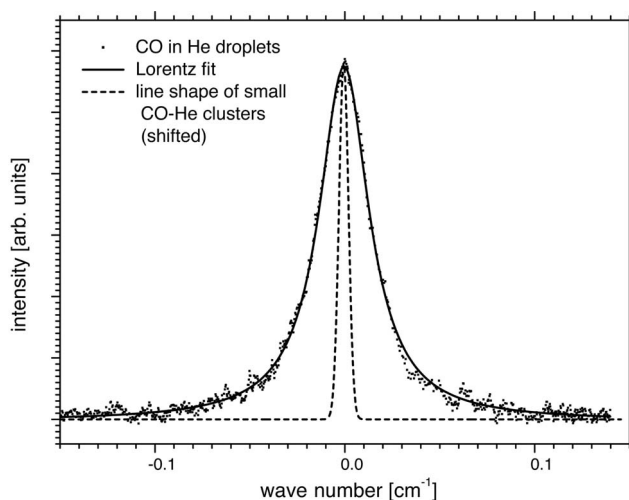


FIG. 14. The $R(0)$ absorption line profile of $^{12}\text{C}^{16}\text{O}$ in large He droplets ($\bar{N}=2600$), compared with the corresponding profile measured in $\text{CO}-(\text{He})_N$ small clusters ($N=2-20$) (Refs. 30 and 32). A fit of the Lorentzian-shaped large droplet spectrum yields a FWHM linewidth of 0.034 cm^{-1} . The linewidth of 0.0033 cm^{-1} for small clusters was taken from Refs. 31 and 32. This small cluster value is limited by the spectral width of the laser source. For better comparison of the line shape, the spectral frequency of CO in small clusters has been shifted to the transition frequency observed here in large droplets

is a significant uncertainty of approximately 40% in this estimate as a result of a finite size bias of the simulation box.

The large rotational linewidth for CO can be understood in terms of the potential anisotropy. For comparison with HCN, we can estimate an upper limit of the homogeneous linewidth from the rovibrational spectrum of HCN in Ref. 27 [on the order of $\sim 0.0067\text{ cm}^{-1}$ (FWHM)] which corresponds to a rotational relaxation time on the order of $8 \times 10^{-10}\text{ s}$. Microwave saturation experiments of HCN yielded a rotational relaxation time of the order of 10^{-8} s which corresponds to a linewidth of $\sim 0.0005\text{ cm}^{-1}$ (FWHM).⁷⁶ In both cases the linewidth is much smaller than for CO [0.034 cm^{-1} (exp.) and 0.018 cm^{-1} (CBF)], despite the similar value of B_{eff} for the two molecules. The vastly different linewidth for CO and the more symmetric HCN molecule is a consequence of the different symmetry contributions to $g(r, \cos\theta)$: according to Eq. (2.6), only the square of the dipole coefficient, $g_1^2(k)$, of the pair distribution contributes to the homogeneous rotational linewidth. Due to the large asymmetry of the $\text{CO}-^4\text{He}$ interaction, $g_1^2(k)$ is large for CO, significantly larger than for HCN as is shown in Fig. 11. The completely symmetric HCCH molecule provides an extreme case of this trend. Here the rotational linewidth of the $R(0)$ transition vanishes in CBF theory, which is a direct consequence of the vanishing of $g_1^2(k)$ for this molecule.³⁰

We point out again that our CBF/DMC calculation for CO in bulk helium obviously cannot quantify the contribution of ripplon excitations to line broadening (see Sec. II B 2). Although ripplon wave functions decay exponentially with a distance from the surface, the experimentally accessible droplet sizes are too small to unambiguously rule out cou-

pling to ripples. The smaller linewidth of the CBF/DMC calculation (i.e., with phonon coupling only) compared to the experimental line width could, therefore, indicate an unaccounted contribution from ripples. Furthermore, the CBF/DMC calculation yields the rotational spectrum at $T=0\text{ K}$. At the true droplet temperature of $T \approx 0.4\text{ K}$, thermal population of particle-in-a-box states may lead to additional (inhomogeneous) line broadening.

V. CONCLUSIONS

We have measured the rovibrational spectrum of four isotopomers of CO which have been embedded in ^4He droplets, and calculated the corresponding pure rotational spectrum in the limit of bulk liquid ^4He using the CBF/DMC theory. The vibrational shift was found to be $-0.254 \pm 0.07\text{ cm}^{-1}$. The effective rotational constants B_{eff} extracted from the measured rovibrational spectra for droplets with $\bar{N} \geq 2600$ are 63% of the gas-phase value, in good agreement with the calculated CBF/DMC value of 69% for $^{12}\text{C}^{16}\text{O}$ in bulk helium. The $R(0)$ frequency was seen to saturate for droplets with an average size greater than $\bar{N} \sim 2000-2200$. Our calculations for small clusters having approximately two solvation shells, $N=64$, yielded an effective rotational constant value of $B_{\text{eff}}/B_0=77\%$. This value, similar to that calculated by the analogous zero temperature methods for small clusters with $N \sim 20-30$,³⁷ is consistent with the measured ref shift of the $R(0)$ transition for droplets smaller than the critical size (but still larger than one solvation shell), and indicates a very slow convergence of the effective rotational constant to its saturation value for CO in large droplets.

We have also investigated the linewidths of CO-doped He droplets. Experimentally, the FWHM linewidths of 0.034 cm^{-1} for the largest droplet sizes were found to be independent of the isotopic constitution and at least an order of magnitude larger than the linewidths measured recently in very small $\text{CO}-(^4\text{He})_N$ clusters. The line shapes were also seen to be broader and asymmetric and exhibit a size dependence for smaller droplets, while for droplets larger than the same critical size $\bar{N} \sim 2000-2200$ as for the $R(0)$ frequency, line shapes converge to a Lorentzian shape, indicating homogeneous broadening.

We have analyzed the origin of the reduction of the B constant and the line broadening by means of the CBF/DMC theory for CO in bulk helium. This gave rise to recognition of the key feature of coupling of the CO rotation to collective modes of the helium, which was seen to be responsible for both the reduction in B constant and the line broadening in large droplets. These calculations reveal that in bulk the $J=1$ state of CO can relax by excitation of a phonon of approximately $\lambda=30\text{ \AA}$. Direct coupling between CO rotation and a long-wavelength collective mode is absent in the small clusters studied recently by Tang and McKellar.^{31,32} We argue that the fact that these cannot support collective modes of this wavelength account for their narrower linewidths, as well as their larger effective rotational constants. Qualitative arguments were presented to show that in large droplets the molecule couples to a combination of discrete

phonon modes and densely spaced particle-in-a-box states, instead of the coupled continua of collective helium modes and molecular translational modes present in bulk.

Detailed analysis and comparison with similar molecules showed that the coupling strength to phonons is controlled by both the speed of rotation (i.e., the gas-phase B_0 value) and the anisotropy of the intermolecular potential. A large anisotropy of the molecule-helium potential will increase the coupling to the cloud of virtual phonons dragged by the rotating molecule (which can be considered as the “handle” to excite the phonons) and will increase the coupling strength. In the particular case of CO, the anisotropy is seen to be unusually large and to be responsible for the relatively large reduction of B_{eff} and the larger linewidth compared to other light molecules in He droplets such as HCN. More theoretical work is required, however, for quantitative explanation of the linewidth in finite droplets. Such theoretical studies as well as the experimental study of other molecules will provide a more complete picture of the new finite size effects on molecular coupling to collective modes in

superfluid helium that are revealed by the current study of CO in helium droplets.

ACKNOWLEDGMENTS

We are grateful for the help of I. Scheele during the construction period of the experimental apparatus, for the help by Andreas Rüdiger and Carsten Krause recording infrared spectra, and for useful hints and calculations on the excluded volume model by Carlo Callegari. The authors would like to acknowledge support by the DFG under Grant Nos. HA 2394/3-1 and HA 2394/9-3 within the *Schwerpunktprogramm SPP1116*. I. S. thanks the DFG for financial support under Grant No. 436 RUS 113/608/0 during his visit to Bochum. This work was also supported by the Miller Institute for Basic Research in Science (R. E. Z.) and by the NSF under Grant No. CHE-010754. The authors would like to thank the Central Information Services of the Johannes Kepler University, Linz, for providing computational resources.

*Email address: Klaus.von.Haeften@rub.de

†Permanent address: General Physics Institute RAS, ul. Vavilova 38, 119991 Moscow, Russia.

- ¹J. Wilks and D. S. Betts, *An Introduction to Liquid Helium* (Clarendon Press, New York, 1987).
- ²L. Landau, *J. Phys. (USSR)* **5**, 185 (1941).
- ³L. Landau, *J. Phys. (USSR)* **11**, 205 (1947).
- ⁴R. A. Cowley and A. D. B. Woods, *Can. J. Phys.* **49**, 177 (1971).
- ⁵R. J. Donnelly, *Quantized Vortices in Helium II* (Cambridge University Press, Cambridge, (1991).
- ⁶K. B. Davis, M. O. Mewes, M. R. Andrews, N. J. van Druten, D. S. Durfee, D. M. Kurn, and W. Ketterle, *Phys. Rev. Lett.* **75**, 3969 (1995).
- ⁷M. E. Gehm, S. L. Hemmer, S. R. Granade, K. M. O’Hara, and J. E. Thomas, *Phys. Rev. A* **68**, 011401(R) (2003); J. Kinast, A. Turlapov, and J. E. Thomas, *ibid.* **70**, 051401(R) (2004).
- ⁸M. Bartenstein, A. Altmeyer, S. Riedl, S. Jochim, C. Chin, J. H. Denschlag, and R. Grimm, *Phys. Rev. Lett.* **92**, 203201 (2004).
- ⁹J. Jortner and M. Rosenblit, *Adv. Chem. Phys.* **132**, 247 (2006).
- ¹⁰K. W. Madison, F. Chevy, W. Wohlleben, and J. Dalibard, *Phys. Rev. Lett.* **84**, 806 (2000).
- ¹¹J. R. Abo-Shaer, C. Raman, J. M. Vogels, and W. Ketterle, *Science* **292**, 476 (2001).
- ¹²C. Raman, J. R. Abo-Shaer, J. M. Vogels, K. Xu, and W. Ketterle, *Phys. Rev. Lett.* **87**, 210402 (2001).
- ¹³S. Stringari, *Phys. Rev. Lett.* **77**, 2360 (1996).
- ¹⁴F. Dalfovo and S. Stringari, *J. Chem. Phys.* **115**, 10078 (2001).
- ¹⁵Y. Kwon, P. Huang, M. V. Patel, D. Blume, and K. B. Whaley, *J. Chem. Phys.* **113**, 6469 (2000).
- ¹⁶E. Krotscheck and R. E. Zillich, *J. Chem. Phys.* **115**, 10161 (2001).
- ¹⁷M. V. Rama Krishna and K. B. Whaley, *J. Chem. Phys.* **93**, 6738 (1990).
- ¹⁸S. A. Chin and E. Krotscheck, *Phys. Rev. B* **52**, 10405 (1995).
- ¹⁹M. Hartmann, F. Mielke, J. P. Toennies, A. F. Vilesov, and G.

- Benedek, *Phys. Rev. Lett.* **76**, 4560 (1996).
- ²⁰V. S. Babichenko and Y. Kagan, *Phys. Rev. Lett.* **83**, 3458 (1999).
- ²¹K. Nauta and R. E. Miller, *J. Chem. Phys.* **115**, 8384 (2001).
- ²²J. P. Toennies and A. F. Vilesov, *Angew. Chem., Int. Ed.* **43**, 2622 (2004).
- ²³S. Grebenev, M. Hartmann, M. Havenith, B. Sartakov, J. P. Toennies, and A. F. Vilesov, *J. Chem. Phys.* **112**, 4485 (2000).
- ²⁴K. K. Lehmann, G. Scoles, *Science* **279**, 2065 (1998).
- ²⁵C. Callegari, K. K. Lehmann, R. Schmied, and G. Scoles, *J. Chem. Phys.* **115**, 10090 (2001).
- ²⁶Y. Kwon and K. B. Whaley, *Phys. Rev. Lett.* **83**, 4108 (1999).
- ²⁷K. Nauta and R. E. Miller, *Phys. Rev. Lett.* **82**, 4480 (1999).
- ²⁸M. V. Patel, A. Viel, F. Paesani, P. Huang, and K. B. Whaley, *J. Chem. Phys.* **118**, 5011 (2003).
- ²⁹R. E. Zillich and K. B. Whaley, *Phys. Rev. B* **69**, 104517 (2004).
- ³⁰R. E. Zillich, Y. Kwon, and K. B. Whaley, *Phys. Rev. Lett.* **93**, 250401 (2004).
- ³¹J. Tang and A. R. W. McKellar, *J. Chem. Phys.* **119**, 754 (2003).
- ³²A. R. W. McKellar, *J. Chem. Phys.* **121**, 6868 (2004).
- ³³T. G. A. Heijmen, R. Moszynski, P. E. S. Wormer, and A. van der Avoird, *J. Chem. Phys.* **107**, 9921 (1997).
- ³⁴F. Paesani and F. A. Gianturco, *J. Chem. Phys.* **116**, 10170 (2002).
- ³⁵F. Paesani, F. A. Gianturco, M. Lewerenz, and J. P. Toennies, *J. Chem. Phys.* **111**, 6897 (1999).
- ³⁶F. A. Gianturco, M. Lewerenz, F. Paesani, and J. P. Toennies, *J. Chem. Phys.* **112**, 2239 (2000).
- ³⁷P. Cazzato, S. Paolini, S. Moroni, and S. Baroni, *J. Chem. Phys.* **120**, 9071 (2004).
- ³⁸R. E. Zillich, F. Paesani, Y. Kwon, and K. B. Whaley, *J. Chem. Phys.* **123**, 114301 (2005).
- ³⁹T. E. Gough, M. Menge, P. A. Rowntree, and G. Scoles, *J. Chem. Phys.* **83**, 4958 (1985).
- ⁴⁰M. Hartmann, R. E. Miller, J. P. Toennies, and A. Vilesov, *Phys.*

- Rev. Lett. **75**, 1566 (1995).
- ⁴¹J. Harms, J. P. Toennies, and F. Dalfovo, Phys. Rev. B **58**, 3341 (1998).
- ⁴²M. Lewerenz, M. Schilling, and J. P. Toennies, Chem. Phys. Lett. **206**, 381 (1993).
- ⁴³D. W. Chandler and G. E. Ewing, J. Chem. Phys. **73**, 4904 (1980).
- ⁴⁴D. W. Chandler and G. E. Ewing, Chem. Phys. **54**, 241 (1981).
- ⁴⁵W. F. Calaway and G. E. Ewing, J. Chem. Phys. **63**, 2842 (1975).
- ⁴⁶C. M. Lindsay, W. K. Lewis, and R. E. Miller, J. Chem. Phys. **121**, 6095 (2004).
- ⁴⁷B. Callicoatt, D. D. Mar, V. A. Apkarian, and K. C. Janda, J. Chem. Phys. **105**, 7872 (1996).
- ⁴⁸M. Lewerenz, M. Schilling, and J. P. Toennies, J. Chem. Phys. **102**, 8191 (1995).
- ⁴⁹K. Nauta and R. E. Miller, Science **283**, 1895 (1999).
- ⁵⁰K. Nauta and R. E. Miller, J. Chem. Phys. **115**, 4508 (2001).
- ⁵¹R. Brügemann, M. Petri, H. Fischer, D. Mauer, D. Reinert, and W. Urban, Appl. Phys. B: Photophys. Laser Chem. **B48**, 105 (1989).
- ⁵²M. Havenith, G. Hilpert, M. Petri, and W. Urban, Mol. Phys. **81**, 1003 (1994).
- ⁵³A. G. Maki and J. S. Wells, "Wavenumber Calibration Tables From Heterodyne Frequency Measurements", 1991, NIST Special Publication 821, U.S. Government Printing Office, Washington.
- ⁵⁴J. P. Toennies and A. F. Vilesov, Chem. Phys. Lett. **235**, 596 (1995).
- ⁵⁵A. R. Janzen and R. A. Aziz, J. Chem. Phys. **107**, 914 (1997).
- ⁵⁶J. Casulleras and J. Boronat, Phys. Rev. B **52**, 3654 (1995).
- ⁵⁷K. Lehmann, Mol. Phys. **97**, 645 (1999).
- ⁵⁸D. M. Ceperley, Rev. Mod. Phys. **67**, 279 (1995).
- ⁵⁹R. K. Bryan, Eur. Biophys. J. **18**, 165 (1990).
- ⁶⁰B. H. Wells, Chem. Phys. Lett. **115**, 89 (1985).
- ⁶¹B. L. Hammond, W. A. Lester, Jr. and P. J. Reynolds, *Monte Carlo Methods in Ab Initio Quantum Chemistry* (World Scientific, Singapore, 1994).
- ⁶²R. N. Barnett and K. B. Whaley, Phys. Rev. A **47**, 4082 (1993).
- ⁶³M. Hartmann, N. Pörtner, B. Sartakov, J. P. Toennies, and A. F. Vilesov, J. Chem. Phys. **110**, 5109 (1999).
- ⁶⁴Carlo Callegari, PhD. thesis, Princeton University (2000).
- ⁶⁵D. Eichenauer and R. J. Le Roy, Phys. Rev. Lett. **57**, 2920 (1986).
- ⁶⁶J. Jortner and N. Ben-Horin, J. Chem. Phys. **98**, 9346 (1993).
- ⁶⁷C. Chackerian, J. Chem. Phys. **65**, 4228 (1976).
- ⁶⁸G. Maroulis *et al.*, J. Phys. Chem. **100**, 13466 (1996).
- ⁶⁹R. J. LeRoy, C. Bissonnette, T. H. Wu, A. K. Dham, and W. J. Meath, Faraday Discuss. **97**, 81 (1994).
- ⁷⁰C. Callegari, A. Conjusteau, I. Reinhard, K. K. Lehmann, G. Scoles, and F. Dalfovo, Phys. Rev. Lett. **83**, 5058 (1999).
- ⁷¹Y. Kwon and K. B. Whaley, J. Chem. Phys. **119**, 1986 (2003).
- ⁷²E. Lee, D. Farrelly, and K. B. Whaley, Phys. Rev. Lett. **83**, 3812 (1999).
- ⁷³K. M. Atkins and J. M. Hutson, J. Chem. Phys. **105**, 440 (1996).
- ⁷⁴R. Moszynski, P. E. S. Wormer, and A. van der Avoird, J. Chem. Phys. **102**, 8385 (1995).
- ⁷⁵K. Higgins and W. Klemperer, J. Chem. Phys. **110**, 1383 (1999).
- ⁷⁶A. Conjusteau, C. Callegari, I. Reinhard, K. K. Lehmann, and G. Scoles, J. Chem. Phys. **113**, 4840 (2000).
- ⁷⁷S. Grebenev, M. Havenith, F. Madeja, J. P. Toennies, and A. F. Vilesov, J. Chem. Phys. **113**, 9060 (2000).
- ⁷⁸I. Reinhard, C. Callegari, A. Conjusteau, K. K. Lehmann, and G. Scoles, Phys. Rev. Lett. **82**, 5036 (1999).
- ⁷⁹C. Callegari, I. Reinhard, K. K. Lehmann, G. Scoles, K. Nauta, and R. E. Miller, J. Chem. Phys. **113**, 4636 (2000).
- ⁸⁰C. Callegari, A. Conjusteau, I. Reinhard, K. K. Lehmann, and G. Scoles, J. Chem. Phys. **113**, 10535 (2000).
- ⁸¹M. Kunze, P. R. L. Markwick, N. Pörtner, J. Reuss, and M. Havenith, J. Chem. Phys. **116**, 7473 (2002).
- ⁸²R. Fröchtenicht, M. Kaloudis, M. Koch, and F. Huisken, J. Chem. Phys. **105**, 6128 (1996).
- ⁸³K. Nauta and R. E. Miller, J. Chem. Phys. **111**, 3426 (1999).
- ⁸⁴K. Nauta and R. E. Miller, J. Chem. Phys. **113**, 9466 (2000).
- ⁸⁵K. Nauta and R. E. Miller, Chem. Phys. Lett. **350**, 225 (2001).
- ⁸⁶F. Paesani, A. Viel, F. A. Gianturco, and K. B. Whaley, Phys. Rev. Lett. **90**, 073401 (2003).
- ⁸⁷F. Paesani and K. B. Whaley, J. Chem. Phys. **121**, 5293 (2004).
- ⁸⁸F. Paesani and K. B. Whaley, J. Chem. Phys. **121**, 4180 (2004).
- ⁸⁹F. Paesani, Y. Kwon, and K. B. Whaley, Phys. Rev. Lett. **94**, 153401 (2005).
- ⁹⁰S. Grebenev, J. P. Toennies, and A. F. Vilesov, Science **279**, 2083 (1998).
- ⁹¹Jian Tang, Yunjie Xu, A. R. W. McKellar, and W. Jäger, Science **297**, 2030 (2002).
- ⁹²Yunjie Xu, W. Jäger, Jian Tang, and A. R. W. McKellar, Phys. Rev. Lett. **91**, 163401 (2003).
- ⁹³Jian Tang and A. R. W. McKellar, J. Chem. Phys. **121**, 181 (2004).
- ⁹⁴K. Nauta, and R. E. Miller, J. Chem. Phys. **115**, 10254 (2001).
- ⁹⁵S. Paolini, S. Fantoni, S. Moroni, S. Baroni, J. Chem. Phys. **123**, 11430 (2005).
- ⁹⁶M. Behrens, U. Buck, R. Fröchtenicht, M. Hartmann, F. Huisken, and F. Rohmund, J. Chem. Phys. **109**, 5914 (1998).